11

Asymmetric Supercapacitor Assembly and analysis of electrochemical performance

11.1. Introduction

Performance of the prepared carbon-based materials as anodes and zinc cobaltite-based materials as cathodes have been employed for the supercapacitor device assembly in asymmetric configuration. The devices are studied for different electrochemical properties and the results are discussed in detail in this Chapter.

11.2. Asymmetric supercapacitor configuration

In the present work, asymmetric supercapacitor devices were fabricated in following two electrode configurations using the prepared carbon and undoped and doped $ZnCo_2O_4$.

(i) S-Carbon /PVA-KOH/ $ZnCo_2O_4$

(ii) S-Carbon /PVA-KOH/ Fe,Cr: $ZnCo_2O_4$

(iii) S-Carbon /PVA-KOH/ Ni,Cr: $ZnCo_2O_4$

(iv) B-Carbon /PVA-KOH/ $ZnCo_2O_4$

(v) B-Carbon /PVA-KOH/ Fe,Cr: $ZnCo_2O_4$

(vi) B-Carbon /PVA-KOH/ Ni,Cr: $ZnCo_2O_4$

(vii) PB-Carbon /PVA-KOH/ $ZnCo_2O_4$

(viii) PB-Carbon /PVA-KOH/ Fe,Cr: $ZnCo_2O_4$

(ix) PB-Carbon /PVA-KOH/ Ni,Cr: $ZnCo_2O_4$

11.2.1. Electrochemical performance of asymmetric device with the configuration of S-Carbon with undoped and doped $ZnCo_2O_4$

The Cyclic voltammetric analysis of asymmetric device assembled with S-Carbon Vs $ZnCo_2O_4$, S-Carbon Vs Fe,Cr:$ZnCo_2O_4$ and S-Carbon Vs Ni,Cr:$ZnCo_2O_4$ are shown in Figure 91a, 91b and 91c. In all the devices, the PVA-KOH electrolyte is used as electrolyte.

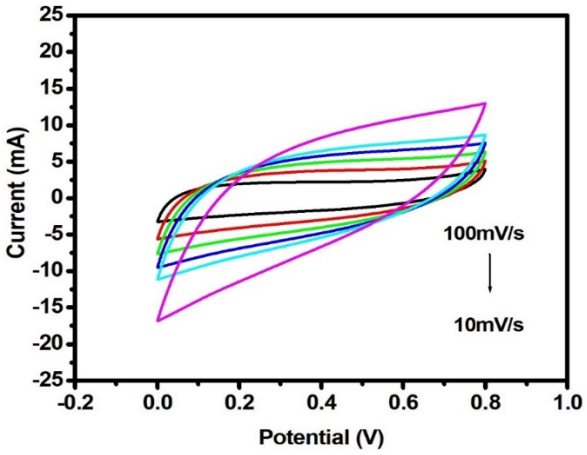

Figure 91a - Cyclic voltammogram of S-Carbon/PVA-KOH/$ZnCo_2O_4$ device

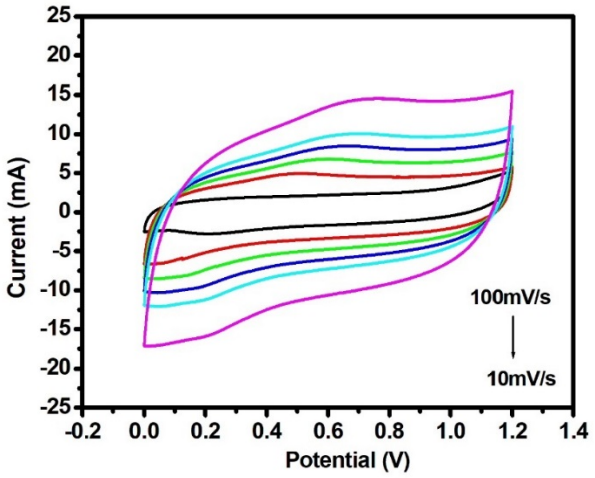

Figure 91b - Cyclic voltammogram of S-Carbon/PVA-KOH/Fe,Cr:$ZnCo_2O_4$ device

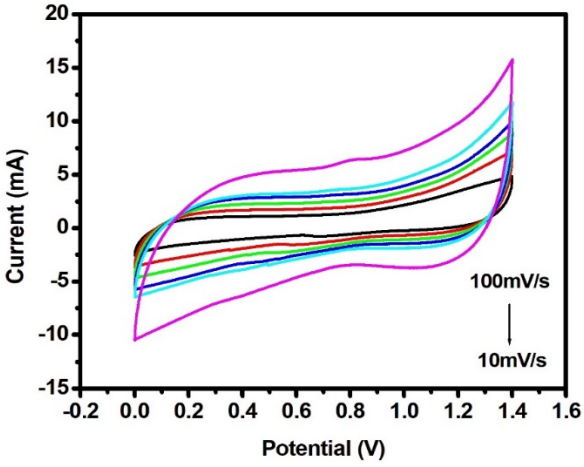

Figure 91c - Cyclic voltammogram of S-Carbon/PVA-KOH/Fe,Cr:$ZnCo_2O_4$ device

The potential window of the asymmetric device is fixed considering the facts: (i) stable electrochemical potential window of all the counterparts included in the device and (ii) suitability of electrode with electrolyte material. After optimization, the working potential window of the device S-Carbon /PVA-KOH/ $ZnCo_2O_4$ is fixed between 0 to 0.8V, for S-Carbon Vs Fe,Cr:$ZnCo_2O_4$ is 0V -1.2V and for S-Carbon Vs Ni,Cr:$ZnCo_2O_4$ is 0V- 1.4V respectively.

Optimizing the performance of the asymmetric device is critical for achieving high energy density. It's worth noting that in asymmetric mode the applied voltage is distributed evenly between the two electrodes. However, the behaviour of the two electrodes are different in nature and the voltage is splitted, based on the capacitance of each electrode. It is proportional to its mass and capacitance. Hence, the mass of the two electrodes are balanced by using the theory of charge balance ($q^+=q^-$):

$$q = C_m \Delta V m \tag{12}$$

$$\frac{m_+}{m_-} = \frac{C_- V_-}{C_+ V_+} \tag{13}$$

C_m – specific capacitance of the electrode, ΔV – potential window and m- mass of the electrode.

Here, C_- and V_- are the potential window and the specific capacitance of the S-Carbon and the values are 0.7 V and 84 Fg^{-1} as explained in Chapter 4. For S-Carbon//$ZnCo_2O_4$ device, C_+ and V_+ are 0.5V and 266 Fg^{-1} as given in Chapter 7. In the case of S-Carbon//Fe,Cr:$ZnCo_2O_4$ device, C_+ and V_+ values are 0.5V and 320 Fg^{-1} as explained in Chapter 8 and finally, C_+ and V_+ for S-Carbon//Ni,Cr:$ZnCo_2O_4$ device are 0.6V and 575 Fg^{-1} as described in Chapter 9. Based on this, the calculated mass ratio of the S-Carbon /PVA-KOH/ $ZnCo_2O_4$, S-Carbon /PVA-KOH/ Fe,Cr:$ZnCo_2O_4$ and S-Carbon /PVA-KOH/ Ni,Cr:$ZnCo_2O_4$ are 0.44,0.36 and 0.17 respectively.

The CV curves of 91a, 91b and 91c have a deviated rectangular shape indicating existence of both EDLC and pseudocapacitive behaviour. The mixed behaviour arises due to the EDLC type carbon material and pseudocapacitive type Zinc cobaltite have been used as an anode and cathode in this case. It is verified by the linear plot between the logarithmic value of scan rate versus current at a particular voltage.

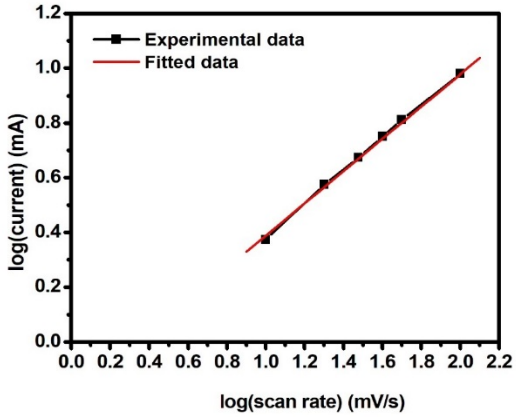

Figure 92a - Power law dependence of charge storage mechanism for S-Carbon/PVA-KOH/$ZnCo_2O_4$ device

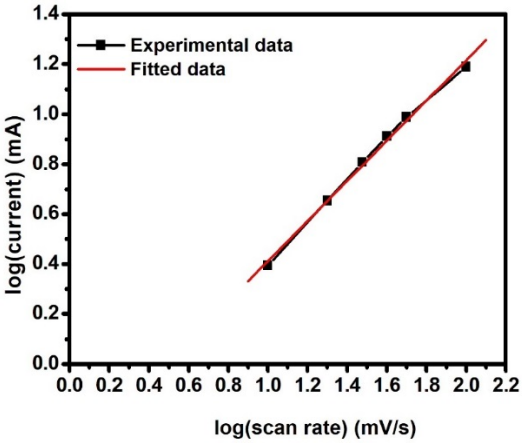

Figure 92b - Power law dependence of charge storage mechanism for S-Carbon /PVA-KOH/ Fe,Cr:$ZnCo_2O_4$ device

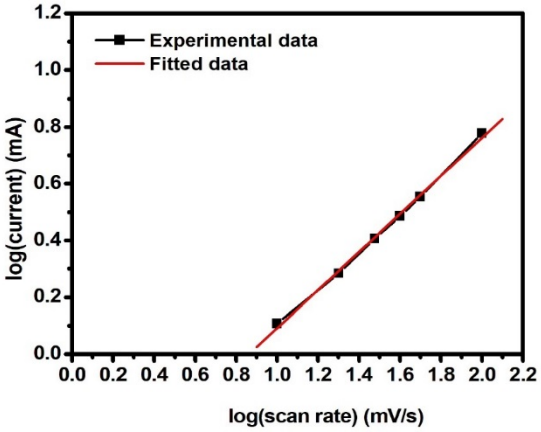

Figure 92c - Power law dependence of charge storage mechanism for S-Carbon /PVA-KOH/ Ni,Cr:$ZnCo_2O_4$ device

It has the slope values of 0.61, suggesting that the fabricated asymmetric device has the slope value of 0.61, 0.80 and 0.73 for S-Carbon Vs $ZnCo_2O_4$, S-Carbon Vs Fe,Cr:$ZnCo_2O_4$ and S-Carbon Vs Ni,Cr:$ZnCo_2O_4$, as shown in Figure 92a, 92b and 92c. Compared to all the slope values, the asymmetric device with configuration of S-Carbon /PVA-KOH/ Fe,Cr:$ZnCo_2O_4$ exhibits higher slope value and is closer to 1 indicating high capacitive behaviour of the device as expected from the half cell performance reported in Chapter 5 (94% of capacitance retention after 2000 cycles).

The complete analysis of this type of behaviour has been made by Using Eq 11, given in the Chapter 10. The co-existence of capacitive and diffusive component in the total current of the CV analysis of the asymmetric device has been separated and the capacitive contribution is marked as a red region in the CV curve at the scan rate of 10 mV/s, Figure 93a, 93b and 93c. The capacitive contribution values for S-Carbon Vs $ZnCo_2O_4$, S-Carbon Vs Fe,Cr:$ZnCo_2O_4$ and S-Carbon Vs Ni,Cr:$ZnCo_2O_4$ asymmetric devices are 42%, 56% and 40% respectively. The device fabricated with S-Carbon /PVA-KOH/ Fe,Cr:$ZnCo_2O_4$ shows higher capacitive contribution as expected from the linear plot when compared with other two devices.

GCD analysis has been carried out to estimate the capacitive behaviour of the S-Carbon /PVA-KOH/ $ZnCo_2O_4$, S-Carbon /PVA-KOH/ Fe,Cr:$ZnCo_2O_4$, and S-Carbon /PVA-KOH/ Ni,Cr:$ZnCo_2O_4$, asymmetric device. It is analysed by various current densities from 0.75 Ag^{-1} to 2 Ag^{-1} and the corresponding GCD profile is shown in Figure 94a, 94b and 94c. The distorted GCD curve from the perfect triangular shape indicates that the device has both EDLC and pseudocapacitive contribution in the charge storage mechanism of all three devices and well agrees with the CV analysis of these devices. Compared to the device employed with pristine $ZnCo_2O_4$, and Fe,Cr: $ZnCo_2O_4$ devices, the discharge time of the device with Ni and Cr doped Zinc cobaltite//S-carbon is higher which has increased the area under the GCD curve. The parameters calculated from the GCD analysis of the S-Carbon /PVA-KOH/ $ZnCo_2O_4$, S-Carbon /PVA-KOH/ Fe,Cr:$ZnCo_2O_4$, and S-Carbon /PVA-KOH/ Ni,Cr:$ZnCo_2O_4$ is shown in Table 43. From the table, compared to all fabricated asymmetric device S-Carbon /PVA-KOH/ Ni,Cr:$ZnCo_2O_4$ asymmetric device exhibits higher specific capacitance, energy density and power density of 61.07 Fg^{-1}, 16.62 Wh Kg^{-1} and 1730.62 W Kg^{-1} at the current density of 1 Ag^{-1}.

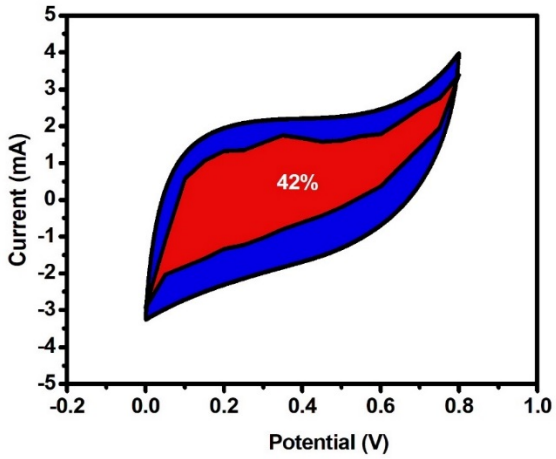

Figure 93a - Capacitive contribution of S-Carbon /PVA-KOH/ $ZnCo_2O_4$ device

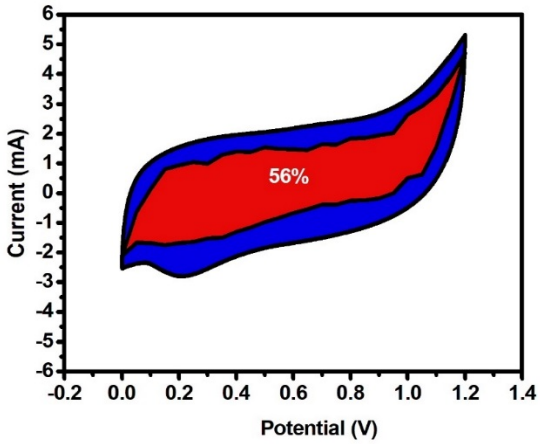

Figure 93b - Capacitive contribution of S-Carbon /PVA-KOH/ Fe,Cr:$ZnCo_2O_4$ device

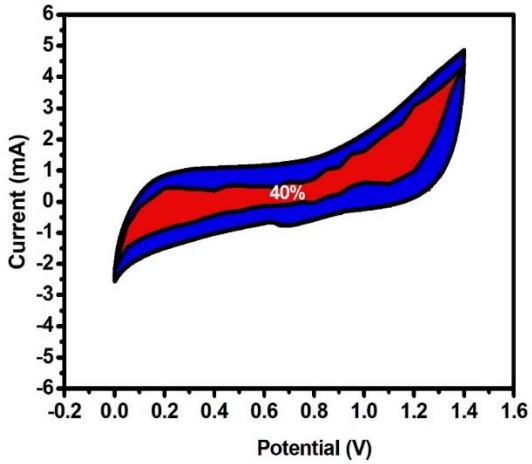

Figure 93c - Capacitive contribution of S-Carbon /PVA-KOH/ Ni,Cr:$ZnCo_2O_4$ device

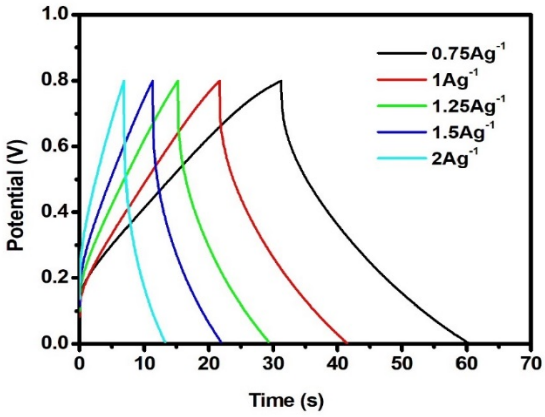

Figure 94a - Galvanostatic Charge-Discharge curves of S-Carbon /PVA-KOH/ $ZnCo_2O_4$ device

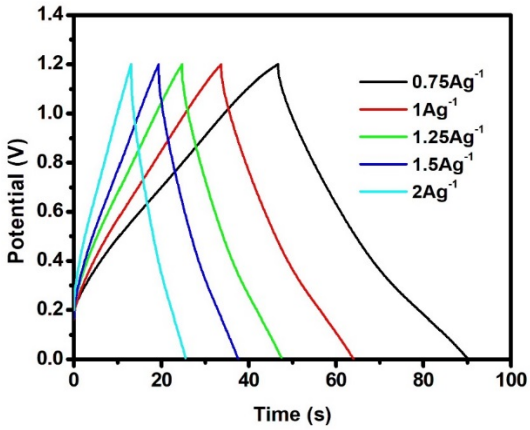

Figure 94b - Galvanostatic Charge-Discharge curves of S-Carbon /PVA-KOH/ Fe,Cr:$ZnCo_2O_4$ device

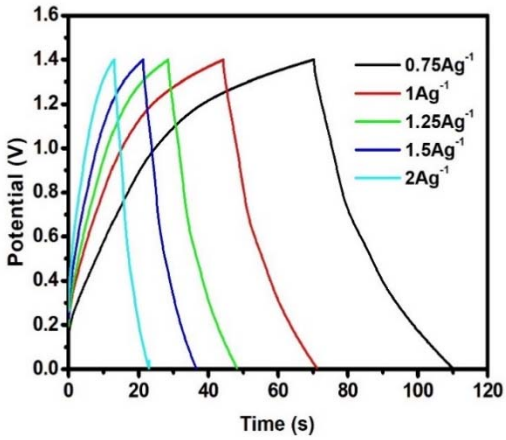

Figure 94c - Galvanostatic Charge-Discharge curves of S-Carbon /PVA-KOH/ Ni,Cr:$ZnCo_2O_4$ device

Table 43 - Gravimetric and areal performance of asymmetric supercapacitor devices of S-Carbon with undoped and doped $ZnCo_2O_4$

Device	Current density ($A\ g^{-1}$)	Specific capacitance ($F\ g^{-1}$)	Specific energy density $WhKg^{-1}$	Specific power density (WKg^{-1})	Areal capacitance ($mF\ cm^{-2}$)	Areal energy density $\mu Wh/cm^2$	Areal power density $\mu W/cm^2$
S-Carbon /PVA-KOH/ $ZnCo_2O_4$	0.75	56.13	4.98	641.51	176.81	15.71	2020.78
	1	49.40	4.39	790.50	155.62	13.83	2490.07
	1.25	43.75	3.88	933.33	137.81	12.25	2940.00
	1.5	39.18	3.48	1140.00	123.44	10.97	3591.00
	2	31.75	2.82	1451.42	100.01	8.89	4572.00
S-Carbon /PVA-KOH/ Fe,Cr:$ZnCo_2O_4$	0.75	57.81	11.56	946.02	190.78	38.15	3121.87
	1	54.44	10.88	1306.66	179.66	35.93	4312.00
	1.25	50.69	10.13	1586.95	167.29	33.45	5236.95
	1.5	47.50	9.50	1900.00	156.75	31.35	6270.00
	2	43.38	8.67	2403.07	143.18	28.63	7930.15
S-Carbon /PVA-KOH/ Ni,Cr:$ZnCo_2O_4$	**0.75**	**70.63**	**19.22**	**1730.62**	**150.10**	**40.86**	**3677.57**
	1	61.07	16.62	2063.79	129.77	35.32	4385.56
	1.25	49.69	13.52	2213.63	105.59	28.74	4703.97
	1.5	45.45	12.37	2801.88	96.60	26.29	5954.00
	2	37.87	10.31	3374.54	80.48	21.91	7170.90

These values are compared with reported articles. A comparative analysis for the electrochemical performance of the previously reported articles of asymmetric device constructed with commercial activated carbon as an anode and Zinc cobaltite material as a cathode is given in Table 44. The lower performance seen in the present case may be attributed to the difference performance of carbon, morphology of $ZnCo_2O_4$ and the choice of current collectors.

Cyclic stability is a key factor to determine the performance of the device. The cyclic stability of S-Carbon /PVA-KOH/ $ZnCo_2O_4$, S-Carbon /PVA-KOH/ Fe,Cr:$ZnCo_2O_4$ and S-Carbon /PVA-KOH/Ni,Cr:$ZnCo_2O_4$, asymmetric devices are tested over 500 cycles at the current density of 3 Ag^{-1}. After 500 cycles, it shows the capacitance retention of 43%, 72% and 77%, in Figure 95a, 95b and 95c. The ASC fabricated using Ni,Cr:$ZnCo_2O_4$ sample as cathode shows 77% capacitance retention after 500 cycles which is higher than the other two cathodes. Hence incorporation of Ni enhances the structural stability of the cathode material resulting in appreciable cyclability.

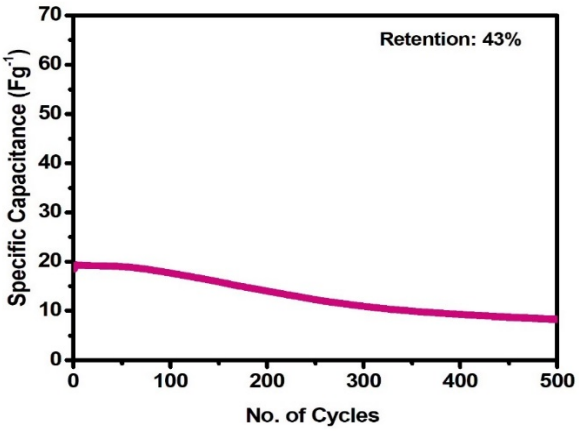

Figure 95a - Cyclic stability of S-Carbon /PVA-KOH/ $ZnCo_2O_4$ device

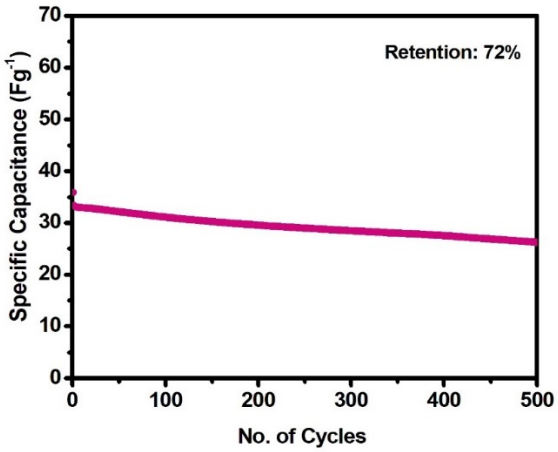

Figure 95b - Cyclic stability of S-Carbon /PVA-KOH/ Fe,Cr:$ZnCo_2O_4$ device

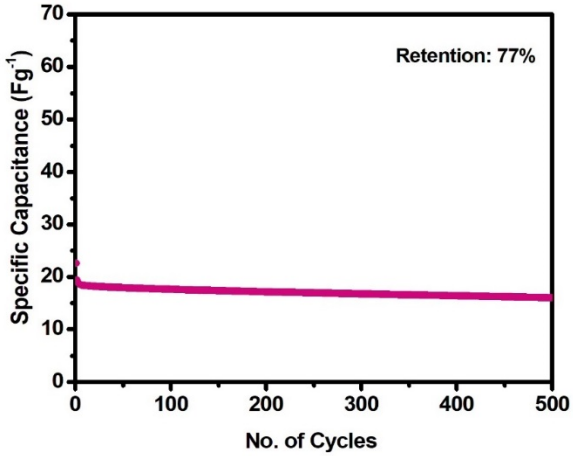

Figure 95c - Cyclic stability of S-Carbon /PVA-KOH/ Ni,Cr:$ZnCo_2O_4$ device

Table 44 - Comparison of Energy and Power density of fabricated asymmetric device using prepared carbon with various literature

S.No	Material and method of preparation	Performance of asymmetric supercapacitor assembly			References
		Configuration	Energy density (Wh Kg^{-1})	Power density (WKg^{-1})	
1.	$ZnCo_2O_4$ and combustion method.	Asymmetric device: Anode: Activated carbon Cathode: $ZnCo_2O_4$@MnO_2 Electrolyte: KOH	26.28 at 1 Ag^{-1}	716	**Bhagwan et al., (2020)**
2.	$ZnCo_2O_4$ and simple hydrothermal method	Asymmetric device: Anode: Activated carbon Cathode: $ZnCo_2O_4$, Electrolyte: KOH	69.2 at 1 Ag^{-1}	774.6	**Du et al., (2020)**
3.	$ZnCo_2O_4$@$CoMoO_4$ core-shell nanosheet arrays Hydrothremal method	Asymmetric device: Anode: Activated carbon Cathode:$ZnCo_2O_4$@$CoMoO_4$ Electrolyte: KOH	29.24 at 1 Ag^{-1}	884.57	**Meng et al., (2020)**
4.	$ZnCo_2O_4$ @$ZnWO_4$ and facile two-step hydrothermal method	Asymmetric device: Anode: Activated carbon Cathode: $ZnCo_2O_4$@ZnWO4 Electrolyte: KOH	24 at 15 mA/cm^2	400	**Xie et al., (2018)**
5.	$ZnCo_2O_4$ and hydrothermal method	Asymmetric device: Anode: Activated carbon Cathode: $ZnCo_2O_4$ Electrolyte: KOH	36.31 Wh Kg^{-1}	850	**Zhu et al., (2018)**
6.	$ZnCo_2O_4$ @MnO_2 and facile hydrothermal method	Asymmetric device: Anode: Activated carbon Cathode: $ZnCo_2O_4$@MnO_2 Electrolyte: PVA- KOH	29.41 at 3 mA/cm^2	628.42	**Yu et al., (2018)**
7.	$ZnCo_2O_4$ and hydrothermal method	Asymmetric device: Anode: Activated carbon Cathode: $ZnCo_2O_4$ Electrolyte: KOH	69 at 0.75 Ag^{-1}	4.9	**Kumbhar & Kim (2018)**
8.	$ZnCo_2O_4$ and facile hydrothermal method	Asymmetric device: Anode: Activated carbon Cathode: $ZnCo_2O_4$, Electrolyte: KOH	45.9 at 1 Ag^{-1}	700	**Chang et al., (2018)**
8.	$ZnCo_2O_4$ and facile Solvothermal method	Asymmetric device: Anode: Activated carbon Cathode: $ZnCo_2O_4$, Electrolyte: KOH	27.78 at 0.2 Ag^{-1}	158.5	**Shang et al., (2018)**

S.No	Material and method of preparation	Performance of asymmetric supercapacitor assembly			References
		Configuration	Energy density (Wh Kg^{-1})	Power density (WKg^{-1})	
9.	$ZnCo_2O_4$ and hydrothermal method	Asymmetric device: Anode: Activated carbon Cathode: $ZnCo_2O_4$/ZnO@MWCNTs Electrolyte: PVA-KOH	48.1 at 0.2 Ag^{-1}	900	**Sun et al., (2017)**
10.	$ZnCo_2O_4$ and simple hydrothermal method	Asymmetric device: Anode: Activated carbon Cathode: $ZnCo_2O_4$ Electrolyte: KOH	33.98 at 1.75 mA/cm^2	8	**Song et al., (2017)**
11.	$ZnCo_2O_4$ and facile hydrothermal method	Asymmetric device: Anode: Activated carbon Cathode: $ZnCo_2O_4$ Electrolyte: PVA-KOH	21.97 at 0.2 Ag^{-1}	38.89	**Gai et al., (2017b)**
12.	$ZnCo_2O_4$ and hydrothermal method	Asymmetric device: Anode: Activated carbon Cathode: $ZnCo_2O_4$ Electrolyte: KOH	13 at 0.5 Ag^{-1}	2997	**Omar et al., (2017)**
13.	$ZnCo_2O_4$@$Ni_xCo_{2x}(OH)_{6x}$ and hydrothermal method	Asymmetric device: Anode: Activated carbon Cathode: $ZnCo_2O_4$@ $Ni_xCo_{2x}(OH)_{6x}$ Electrolyte: KOH	26.2 at 5 mA/cm^2	511.8	**Fu et al., (2015)**

The kinetics of the electrochemical reaction of the fabricated asymmetric devices are investigated by EIS analysis. Figure 96a, 96b and 96c shows the Nyquist plot of S-Carbon /PVA-KOH/ $ZnCo_2O_4$, S-Carbon /PVA-KOH/ Fe,Cr:$ZnCo_2O_4$ and S-Carbon /PVA-KOH/Ni,Cr:$ZnCo_2O_4$ asymmetric devices and the inset shows the corresponding equivalent circuit. The internal resistance R_1 arises due to various parameters such as electrode/electrolyte interface, contact between electrode and current collector and movement of ion into the electrolyte. In all the three devices, the internal resistance is high after cycling which is due to the growth of SEI region on the electrode/electrolyte interface. This resistance directly decreases the capacitance of the device which is true for whole 500 cycles. The fitted parameters are given in Table 45, 46 and 47. In Table 45, after cycling, the n1 value decreases due to the diffusion-controlled process in the fabricated asymmetric

device, it may affect the cyclic stability of the S-Carbon /PVA-KOH/ $ZnCo_2O_4$ device. Also, in S-Carbon /PVA-KOH/ Fe,Cr:$ZnCo_2O_4$ device, after cycling there is a sharp decrement in n2 value, in Table 46. But, in the case of S-Carbon /PVA-KOH/ Ni,Cr: $ZnCo_2O_4$ there is no significant change in n1 and n2 values of before and after cycling which ensures the cyclic stability of the device with Ni,Cr: $ZnCo_2O_4$ cathode.

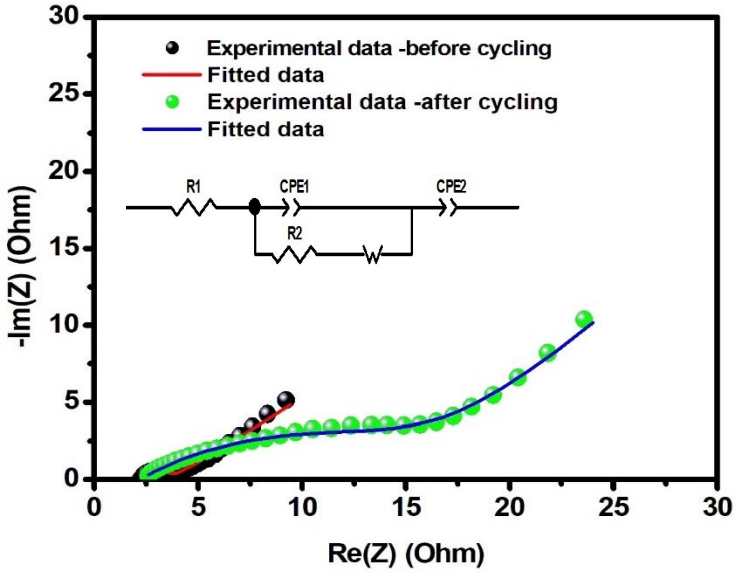

Figure 96a - Electrochemical impedance spectra of S-Carbon /PVA-KOH/ $ZnCo_2O_4$ device

Table 45 - Fitted parameters of electrochemical impedance Spectra of S-Carbon /PVA-KOH/ $ZnCo_2O_4$ device

Parameters	Before Cycling	After Cycling
$R_1(\Omega)$	2.24	2.20
$R_2(\Omega)$	1.16	15.44
CPE 1	0.06×10^{-3}	7.03×10^{-3}
n1	0.91	0.42
CPE 2	0.31	0.13
n2	0.29	0.57
W	5.25	0.57

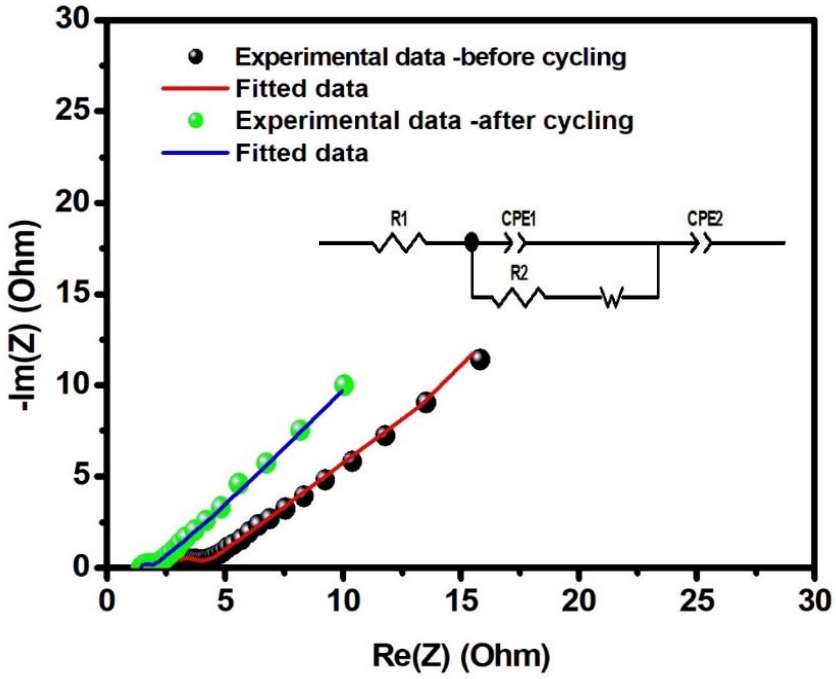

Figure 96b - Electrochemical impedance spectra of S-Carbon /PVA-KOH/ Fe,Cr:$ZnCo_2O_4$ device

Table 46 - Fitted parameters of electrochemical impedance spectra of S-Carbon /PVA-KOH/ Fe,Cr:$ZnCo_2O_4$ device

Parameters	Before Cycling	After cycling
$R_1(\Omega)$	1.44	2.57
$R_2(\Omega)$	0.42	1.33
CPE 1	0.11×10^{-3}	0.25×10^{-3}
n1	0.95	0.79
CPE 2	0.58	0.81
n2	0.84	0.30
W	6.48	8.02

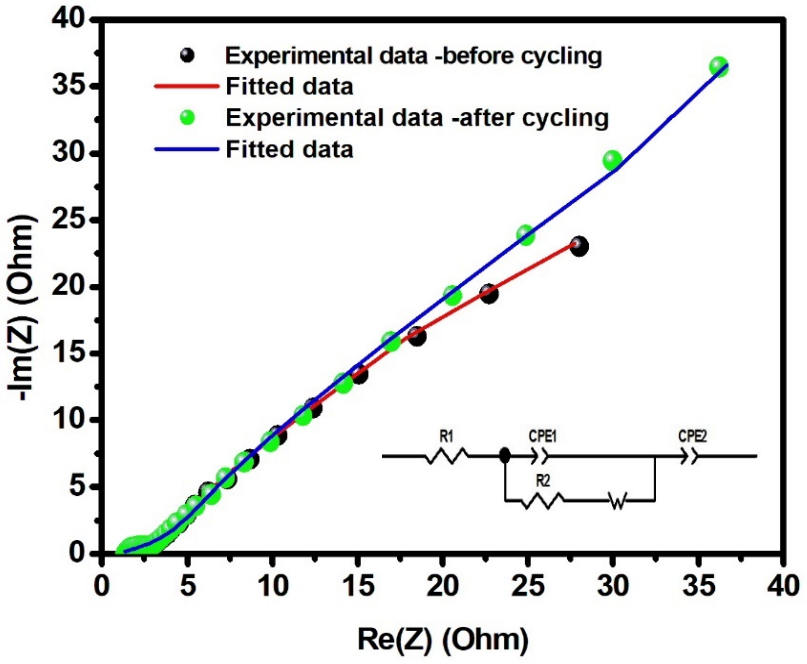

Figure 96c - Electrochemical impedance spectra of S-Carbon /PVA-KOH/ Ni,Cr:$ZnCo_2O_4$ device

Table 47 - Fitted parameters of electrochemical impedance spectra of S-Carbon /PVA-KOH/ Ni,Cr:$ZnCo_2O_4$ device

Parameters	Before Cycling	After Cycling
$R_1(\Omega)$	1.25	0.89
$R_2(\Omega)$	3.90	4.19
CPE 1	0.01	$9.83x10^{-3}$
n1	0.99	0.97
CPE 2	0.16	0.08
n2	0.17	0.23
W	17.32	24.56

11.2.2. Electrochemical performance of asymmetric device with the configuration of B-Carbon with undoped and doped $ZnCo_2O_4$

The asymmetric devices of B-Carbon Vs $ZnCo_2O_4$, B-Carbon Vs Fe,Cr: $ZnCo_2O_4$ and B-Carbon Vs Ni,Cr: $ZnCo_2O_4$ have been fabricated with PVA-KOH electrolyte and tested with a two-electrode system. The operating voltage of the B-Carbon Vs $ZnCo_2O_4$, B-Carbon Vs Fe,Cr: $ZnCo_2O_4$ and B-Carbon Vs Ni,Cr: $ZnCo_2O_4$ asymmetric devices are 0V-0.8V, 0V-1.4V and 0V-1.4V respectively. The optimized mass ratio of above mentioned devices are 1.19, 0.99 and 0.45. The cyclic voltametric analysis of B-Carbon /PVA-KOH/$ZnCo_2O_4$, B-Carbon /PVA-KOH/ Fe,Cr:$ZnCo_2O_4$ and B-Carbon /PVA-KOH/ Ni,Cr:$ZnCo_2O_4$ asymmetric devices are shown in Figure 97a, 97b and 98c.

The deviated rectangular shape seen in Figure 97a, 97b and 97c, similar to that of the pattern observed in previous section. It is analysed by the linear plot which are shown in Figure 98a, 98b and 98c. The calculated b value from the linear plot is 0.52, 0.82 and 0.70 for B-Carbon/PVA-KOH/ $ZnCo_2O_4$, B-Carbon/PVA-KOH/Fe,Cr:$ZnCo_2O_4$ and B-Carbon/PVA-KOH/Ni,Cr:$ZnCo_2O_4$ asymmetric devices. The slope value for B-Carbon Vs Fe,Cr:$ZnCo_2O_4$ and B-Carbon Vs Ni,Cr:$ZnCo_2O_4$ indicating the more capacitive behaviour than B-Carbon Vs $ZnCo_2O_4$. The capacitive contribution is separated from the CV curve of all the three device and the values are 31%, 48% and 54% respectively. The capacitive contributions are indicated as a red region in Figure 99a, 99b and 99c. Fe,Cr:$ZnCo_2O_4$ and Ni,Cr:$ZnCo_2O_4$ devices show faradaic contribution as expected from half cells.

GCD analysis of the B-Carbon /PVA-KOH/ $ZnCo_2O_4$, B-Carbon /PVA-KOH/ Fe,Cr:$ZnCo_2O_4$, and B-Carbon /PVA-KOH/ Ni,Cr:$ZnCo_2O_4$ are given in Figure 100a, 100b and 100c. The distorted GCD curve is supported by CV curve of these devices. In B-Carbon /PVA-KOH/ $ZnCo_2O_4$ asymmetric device, at lower current density, the charging time is very much higher than the discharging time which attributes to the irreversibility of the assembled device. However, the performance of the device is better than the asymmetric device fabricated with S-Carbon Vs Zinc cobaltite. This may be due to the high surface of the B-Carbon employed as an anode material in the fabricated asymmetric device. But, in the case of B-Carbon /PVA-KOH/ Fe,Cr:$ZnCo_2O_4$ device, the charging and discharging times are more identical than other two devices which indicates better reversibility of the device.

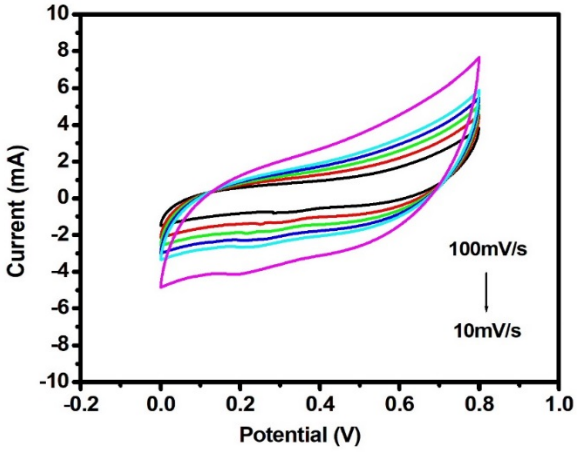

Figure 97a - Cyclic voltammogram of B-Carbon /PVA-KOH/ $ZnCo_2O_4$ device

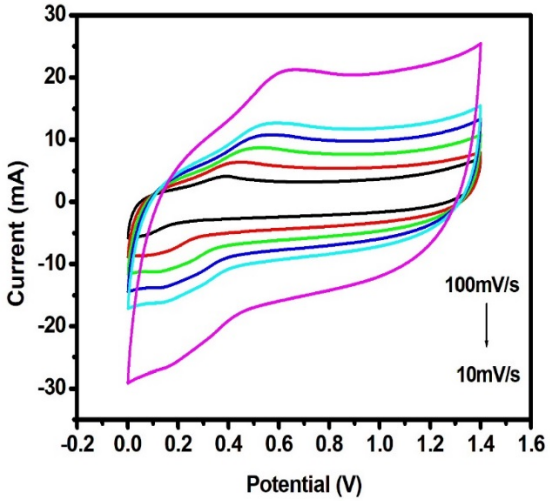

Figure 97b - Cyclic voltammogram of B-Carbon /PVA-KOH/ Fe,Cr:$ZnCo_2O_4$ device

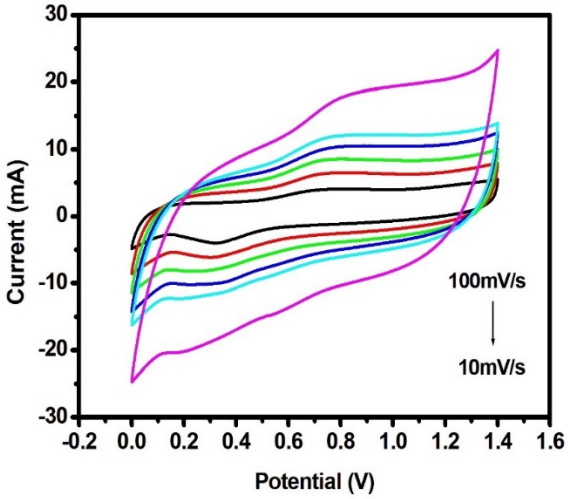

Figure 97c - Cyclic voltammogram of B-Carbon /PVA-KOH/ Ni,Cr:$ZnCo_2O_4$ device

The electrochemical performance calculated from the GCD analysis of the B-Carbon /PVA-KOH/ $ZnCo_2O_4$, B-Carbon /PVA-KOH/ Fe,Cr:$ZnCo_2O_4$, and B-Carbon /PVA-KOH/ Ni,Cr:$ZnCo_2O_4$ is shown in Table 48. Out of all the three asymmetric devices, B-Carbon /PVA-KOH/ Ni,Cr $ZnCo_2O_4$ device exhibits better gravimetric (energy density of 25.00 Wh Kg^{-1} reached at the power density of 1730.76 W Kg^{-1}) as well as areal (areal energy density of 82.50 µWh/cm^2 and 5711.53 µW/cm^2 at 3.3 mA/cm^2) performance than other two devices. The following facts are attributed to the superior performance of B-Carbon /PVA-KOH/ Ni,Cr $ZnCo_2O_4$ (i) high surface area B-Carbon (ii) high specific capacitance Ni,Cr:$ZnCo_2O_4$ (iii) combined performance of electrode materials in a single device. The observed values of B-Carbon /PVA-KOH/ Ni,Cr:$ZnCo_2O_4$ are compared with the reported literature, shown in Table 48. Some reported literature exhibits higher performance than the present work and the corresponding discussions are made in the previous section.

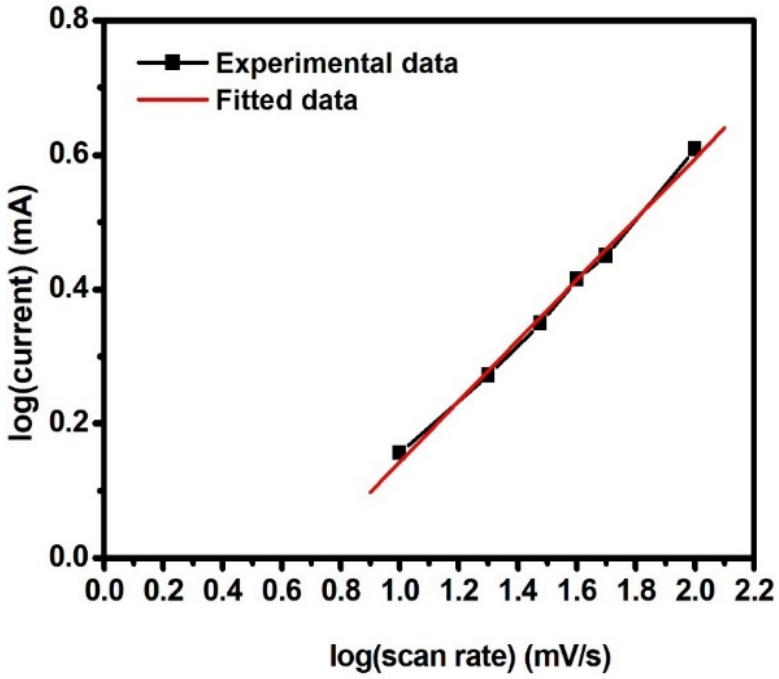

Figure 98a - Power law dependence of charge storage mechanism for B-Carbon /PVA-KOH/ $ZnCo_2O_4$ device

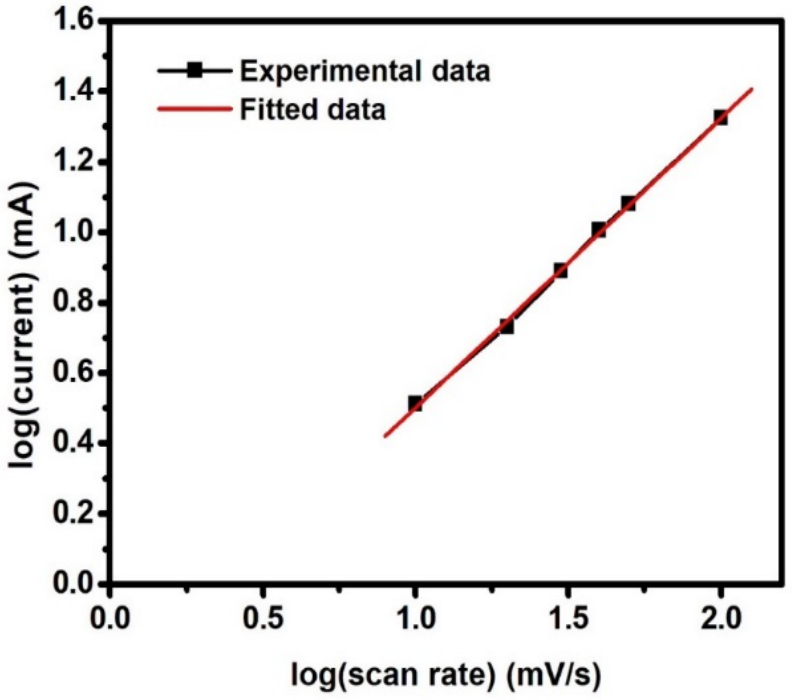

Figure 98b - Power law dependence of charge storage mechanism for B-Carbon /PVA-KOH/ Fe,Cr:$ZnCo_2O_4$ device

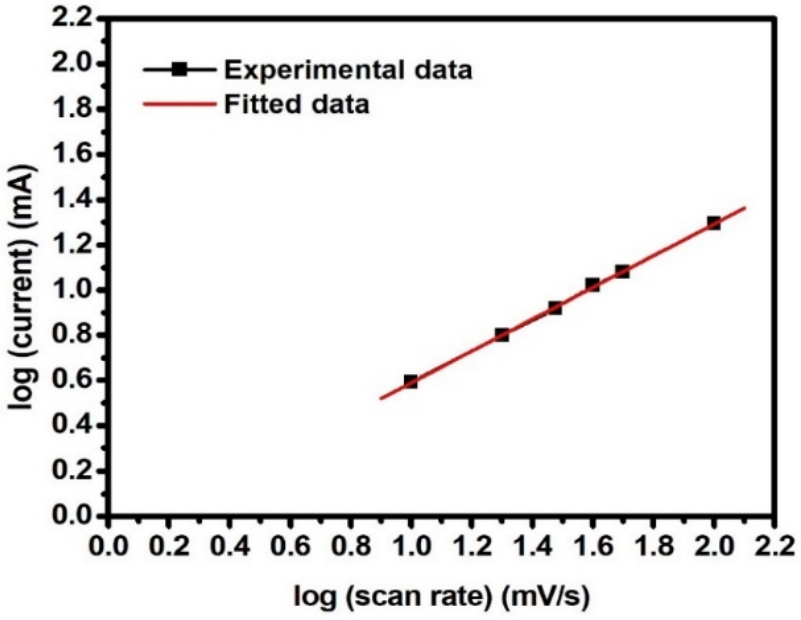

Figure 98c - Power law dependence of charge storage mechanism for B-Carbon /PVA-KOH/ Ni,Cr: $ZnCo_2O_4$ device

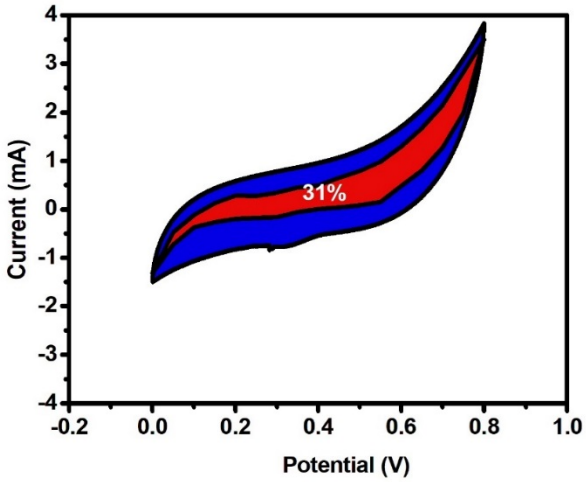

Figure 99a - Capacitive contribution of B-Carbon /PVA-KOH/ $ZnCo_2O_4$ device

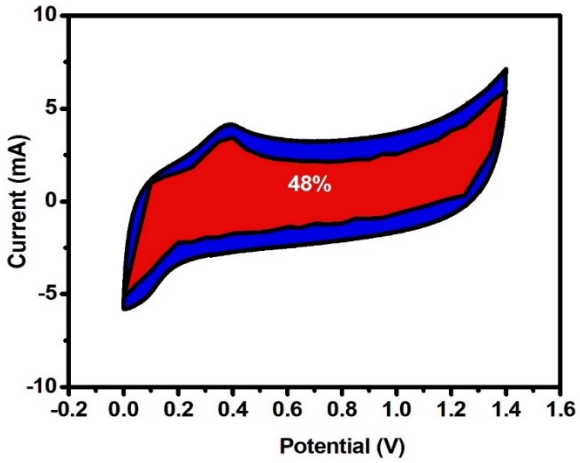

Figure 99b - Capacitive contribution of B-Carbon /PVA-KOH/ Fe,Cr:$ZnCo_2O_4$ device

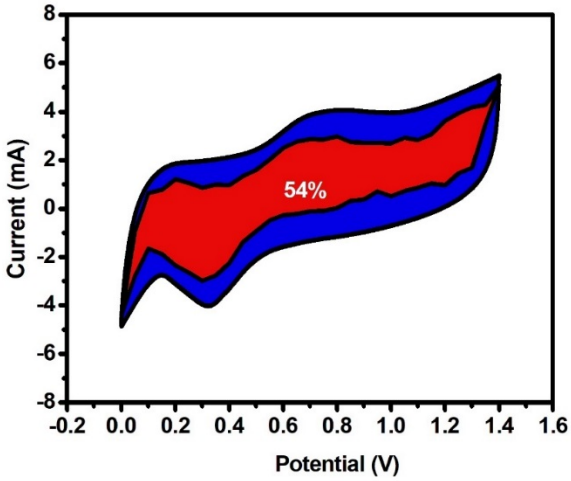

Figure 99c - Capacitive contribution of B-Carbon /PVA-KOH/ Ni,Cr:$ZnCo_2O_4$ device

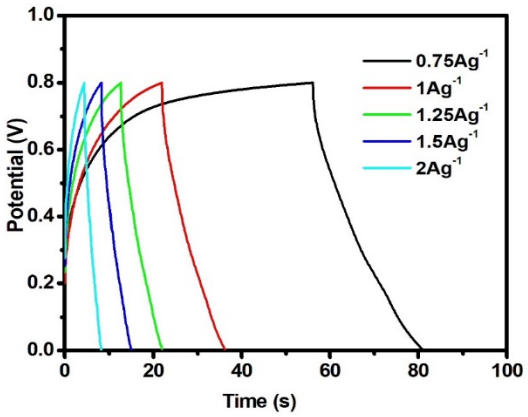

Figure 100a - Galvanostatic Charge-Discharge curves of B-Carbon /PVA-KOH/ $ZnCo_2O_4$ device

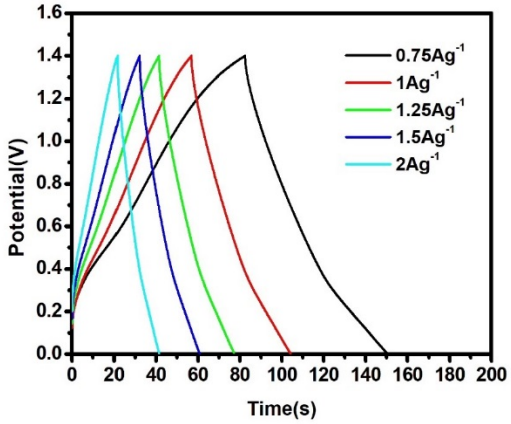

Figure 100b - Galvanostatic Charge-Discharge curves of B-Carbon /PVA-KOH/ Fe,Cr:$ZnCo_2O_4$ device

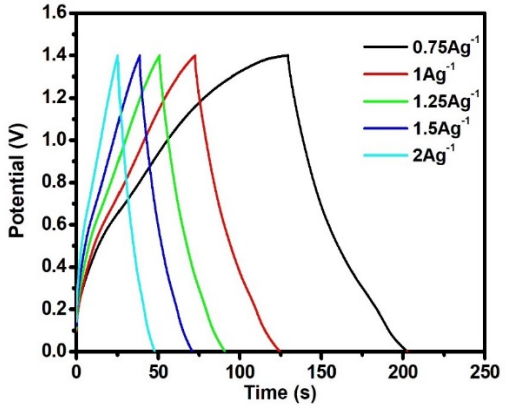

Figure 100c - Galvanostatic Charge-Discharge curves of B-Carbon /PVA-KOH/ Ni,Cr:$ZnCo_2O_4$ device

Table 48 - Gravimetric and areal performance of asymmetric supercapacitor devices of B-carbon with undoped and doped $ZnCo_2O_4$ device

Device	Current density ($A\ g^{-1}$)	Specific capacitance ($F\ g^{-1}$)	Specific energy density $WhKg^{-1}$	Specific power density (WKg^{-1})	Areal capacitance ($mF\ cm^{-2}$)	Areal energy density $\mu Wh/cm^2$	Areal power density $\mu W/cm^2$
B-Carbon /PVA-KOH/ $ZnCo_2O_4$	0.75	110.62	9.83	1416.00	309.75	27.53	3964.80
	1	57.81	5.13	1233.33	161.87	14.38	3453.33
	1.25	42.85	3.80	1371.25	119.98	10.66	3839.50
	1.5	34.35	3.05	1570.71	96.20	8.55	4398.00
	2	24.93	2.21	1900.00	69.82	6.20	5320.00
B-Carbon /PVA-KOH/ Fe,Cr:$ZnCo_2O_4$	0.75	82.63	22.49	1190.95	326.41	88.85	4704.27
	1	74.06	20.16	1544.25	292.54	79.63	6099.80
	1.25	68.62	18.68	1868.05	271.05	73.78	7378.81
	1.5	65.14	17.73	2240.00	257.31	70.04	8848.00
	2	60.40	16.44	2832.53	238.61	64.95	11188.52
B-Carbon /PVA-KOH/ Ni,Cr:$ZnCo_2O_4$	**0.75**	**126.27**	**34.37**	**1695.20**	**416.70**	**113.43**	**5594.17**
	1	91.83	25.00	1730.76	303.06	82.50	5711.53
	1.25	81.63	22.22	1951.22	269.38	73.33	6439.02
	1.5	76.53	20.83	2205.88	252.55	68.75	7279.41
	2	68.57	18.66	2921.73	226.28	61.60	9641.73

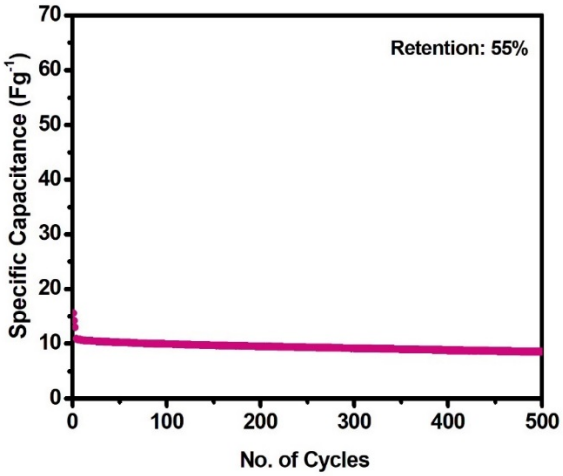

Figure 101a - Cyclic stability of B-Carbon /PVA-KOH/ $ZnCo_2O_4$ device

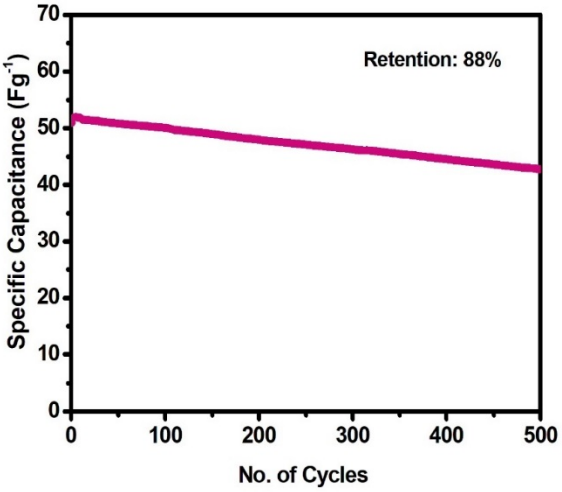

Figure 101b - Cyclic stability of B-Carbon /PVA-KOH/ Fe,Cr:$ZnCo_2O_4$ device

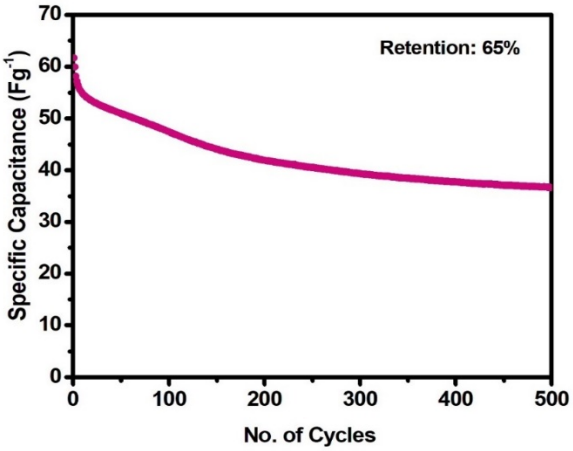

Figure 101c - Cyclic stability of B-Carbon /PVA-KOH/ Ni,Cr:$ZnCo_2O_4$ device

The cyclic stability has been tested for B-Carbon /PVA-KOH/ $ZnCo_2O_4$, B-Carbon /PVA-KOH/ Fe,Cr:$ZnCo_2O_4$ and B-Carbon /PVA-KOH/ Ni,Cr:$ZnCo_2O_4$ asymmetric devices for 500 cycles and the corresponding graphs are shown in Figure 101a, 101b and 101c and the three devices exhibits the capacity retention of 55%, 88% and 65% after 500 cycles respectively. When compared with asymmetric device fabricated with B-Carbon vs pristine and Ni,Cr: $ZnCo_2O_4$, the B-Carbon/PVA-KOH/ Fe,Cr:$ZnCo_2O_4$ asymmetric device shows better cyclic stability which may attributed to the high capacitive contribution in the device.

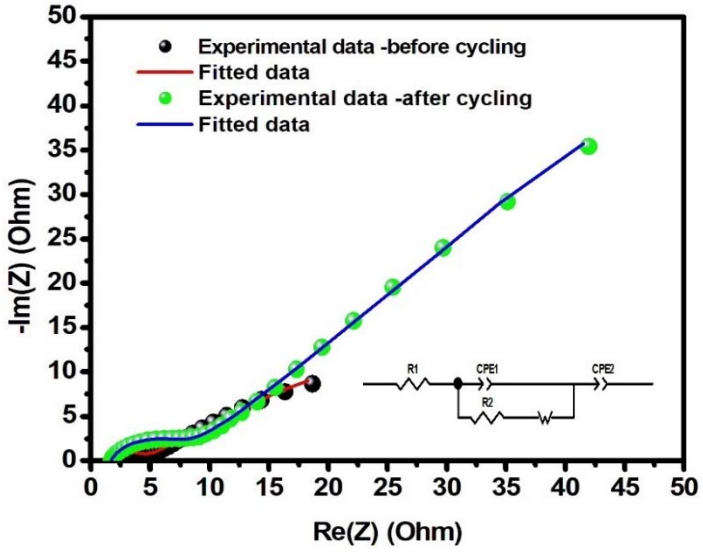

Figure 102a - Electrochemical impedance spectra of B-Carbon /PVA-KOH/ $ZnCo_2O_4$ device

Table 49 - Fitted parameters of electrochemical impedance spectra of B-Carbon/PVA-KOH/ $ZnCo_2O_4$ device

Parameters	Before Cycling	After Cycling
$R_1(\Omega)$	2.17	1.69
$R_2(\Omega)$	1.78	6.28
CPE 1	0.23×10^{-3}	0.39×10^{-3}
n1	0.82	0.76
CPE 2	0.07	0.27
n2	0.36	0.73
W	0.11	24.71

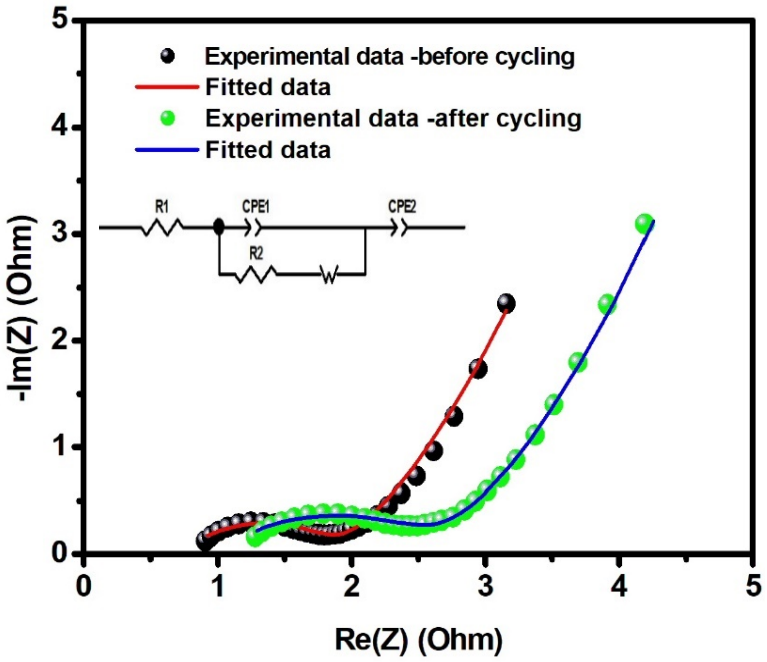

Figure 102b - Electrochemical impedance spectra of B-Carbon /PVA-KOH/ Fe,Cr:$ZnCo_2O_4$ device

Table 50 - Fitted parameters of electrochemical impedance spectra of B-Carbon/PVA-KOH/Fe,Cr :$ZnCo_2O_4$ device

Parameters	Before Cycling	After Cycling
$R_1(\Omega)$	0.72	0.99
$R_2(\Omega)$	1.18	1.68
CPE 1	6.09 $x10^{-3}$	8.31 $x10^{-3}$
n1	0.56	0.50
CPE 2	1.58	1.09
n2	0.98	0.92
W	1.01	1.32

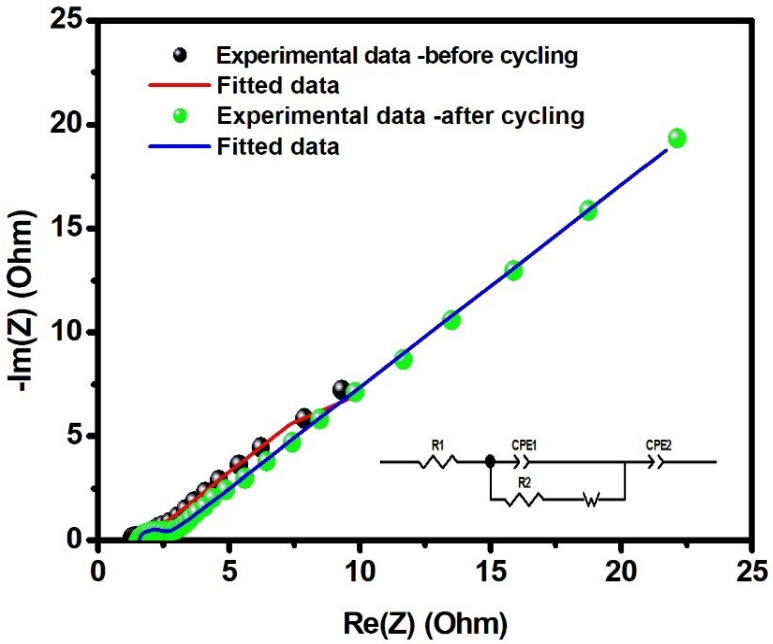

Figure 102c - Electrochemical impedance spectra of B-Carbon /PVA-KOH/ Ni,Cr:$ZnCo_2O_4$ device

Table 51 - Fitted parameters of electrochemical impedance spectra of B-Carbon/PVA-KOH/Ni,Cr:$ZnCo_2O_4$ device

Parameters	Before Cycling	After Cycling
$R_1(\Omega)$	1.26	1.57
$R_2(\Omega)$	0.42	0.86
CPE 1	0.37×10^{-3}	0.04×10^{-3}
n1	0.87	0.99
CPE 2	0.11	0.48
n2	0.49	0.40
W	0.64	13.69

Electrochemical impedance analysis of B-Carbon /PVA-KOH/ $ZnCo_2O_4$, B-Carbon /PVA-KOH/ Fe,Cr:$ZnCo_2O_4$ and B-Carbon /PVA-KOH/ Ni,Cr:$ZnCo_2O_4$ is seen in Figure 102a, 102b and 102c. The plot is fitted with an equivalent circuit using EC lab software and is given as inset image. The fitted parameters are given in Table 49, 50 and 51. In all the three fabricated devices, after cycling, the internal resistance of the asymmetric

device which leads to decrease the cyclic stability of the device. Similar observation has been obtained in the previous case too. But comparing B-Carbon /PVA-KOH/ Fe,Cr:$ZnCo_2O_4$ device with other two devices, device employing with Fe and Cr doped Zinc cobaltite exhibits better cyclic stability due to less increment in internal resistance after cycling for the reasons of electrode/electrolyte interfacial changes as discussed in the half cells in Chapter 8.

11.2.3. Electrochemical performance of asymmetric device with the configuration of PB-Carbon with undoped and doped $ZnCo_2O_4$

The constructed asymmetric supercapacitor device with the configuration of PB-Carbon /PVA-KOH/ $ZnCo_2O_4$, PB-Carbon /PVA-KOH/ Fe,Cr:$ZnCo_2O_4$ and PB-Carbon /PVA-KOH/ Ni,Cr:$ZnCo_2O_4$, have been analysed in this section. The potential window of the PB-Carbon Vs $ZnCo_2O_4$, PB-Carbon Vs Fe,Cr: $ZnCo_2O_4$ and PB-Carbon Vs Ni,Cr: $ZnCo_2O_4$ are fixed and the values are 0V-0.8V, 0V-1.2V and 0V-1.4V respectively**.** Using the equation 14, charge between anode and cathode is optimized by mass ratio of the two electrodes and the corresponding values are 0.48, 0.40 and 0.18 for asymmetric devices fabricated with PB-Carbon anode vs the three metal oxides. The nature of the CV plot has deviated from the rectangular behaviour, which is similar to the asymmetric devices explained in previous sections and the corresponding CV curves are shown in Figure 103a, 103b and 103c. Compared to PB Carbon//$ZnCo_2O_4$, in the case of PB carbon assembled with doped Zinc cobaltite, the shape of the CV curves is well maintained without any deformation even the higher scan rate of 100 mV/s, suggesting the outstanding performance of the device. Moreover, there is no obvious redox peaks are observed. The performance of the device is dominantly capacitive that is verified by the slope value of the linear plot. The slope value obtained from the linear plot for asymmetric devices are shown in Figure 104a, 104b and 104c. The observed slope values are 0.67, 0.92 and 0.88 for PB-Carbon Vs $ZnCo_2O_4$, PB-Carbon Vs Fe,Cr: $ZnCo_2O_4$ and PB-Carbon Vs Ni,Cr: $ZnCo_2O_4$. The slopes of asymmetric device assembled with PB-Carbon anode and doped zinc cobaltite cathode are more close to 1.

For better understanding of the storage mechanism of these devices, using Eq(11), the CV plot is bifurcated at the scan rate of 10 mV/s to know the capacitive contribution of the devices and the value of 50%, 64% and 78% are attained from the total area of the CV

curve for PB-Carbon//$ZnCo_2O_4$, PB-Carbon//Fe,Cr: $ZnCo_2O_4$ and PB-Carbon// Ni,Cr: $ZnCo_2O_4$ respectively which are marked as red region in Figure 105a,105b and 105c. Further, the electrochemical performance is also investigated by GCD measurements at various current densities from 0.75 Ag^{-1} to 3 Ag^{-1}, Figure 106a, 106b and 106c. Compared with PB-Carbon//$ZnCo_2O_4$, PB-Carbon//Fe,Cr: $ZnCo_2O_4$ and PB-Carbon// Ni,Cr: $ZnCo_2O_4$ exhibits triangular shape due to less IR drop/internal resistance, linear relationship between voltage and time, showing more capacitive behaviour. It is due to the incorporation of dopants into pristine Zinc cobaltite and the findings are consistent with the results observed from the CV analysis of PB-Carbon//Fe,Cr: $ZnCo_2O_4$ and PB-Carbon// Ni,Cr: $ZnCo_2O_4$

The gravimetric and areal performance of the fabricated devices with PB-Carbon is tabulated in Table 52. From Table 52, it is clear that PB-Carbon /PVA-KOH/ Ni,Cr:$ZnCo_2O_4$ demonstrates higher energy density 17.37 Wh Kg^{-1} at the power density of 1251.20 W Kg^{-1} and also achieves better areal energy density 72.98 $\mu Wh/cm^2$ with an areal power density of 5255.04 $\mu W/cm^2$. The cyclic stability of the PB-Carbon//$ZnCo_2O_4$, PB-Carbon//Fe,Cr: $ZnCo_2O_4$ and PB-Carbon// Ni,Cr: $ZnCo_2O_4$ device are shown in Figure 107a, 107b and 107c. In PB-Carbon//$ZnCo_2O_4$, only 40% of initial capacitance has been retained after 500 cycles indicating lower cyclic stability of the device. When PB-Carbon is assembled with Fe and Cr doped Zinc cobaltite cathode as well as Ni and Cr doped Zinc cobaltite, the electrochemical stability has improved to 85% and 73% correspondingly.

The electrochemical impedance analysis of PB-Carbon /PVA-KOH/ $ZnCo_2O_4$, PB-Carbon /PVA-KOH/ Fe,Cr:$ZnCo_2O_4$ and PB-Carbon /PVA-KOH/ Ni,Cr: $ZnCo_2O_4$ is shown in Figure 108a, 108b and 108c and equivalent circuit is given in the inset. The obtained fitted parameters are given in Table 53, 54 and 55. In all the three cases, after cycling the internal resistance is increased which is same as that of previous cases. However, the charge transfer resistance rapidly increased for PB-Carbon /PVA-KOH/ $ZnCo_2O_4$ which leads to the capacitance fading (40 % of capacitance retention) after 500 cycles. Both n1 and n2 value of PB-Carbon /PVA-KOH/ $ZnCo_2O_4$ have also decreased which also affects the cyclic stability of the device. In other two cases, there is not much change in charge transfer resistance. Due to the improvement of diffusive behaviour, capacitance loss of 15% and 27% has occurred.

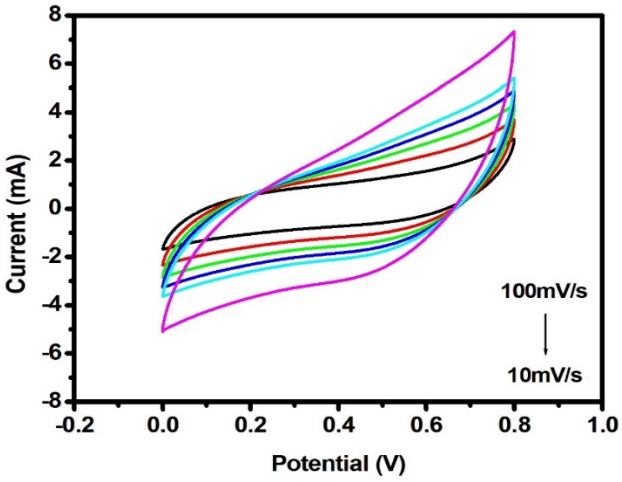

Figure 103a - Cyclic voltammogram of PB-Carbon /PVA-KOH/ $ZnCo_2O_4$ device

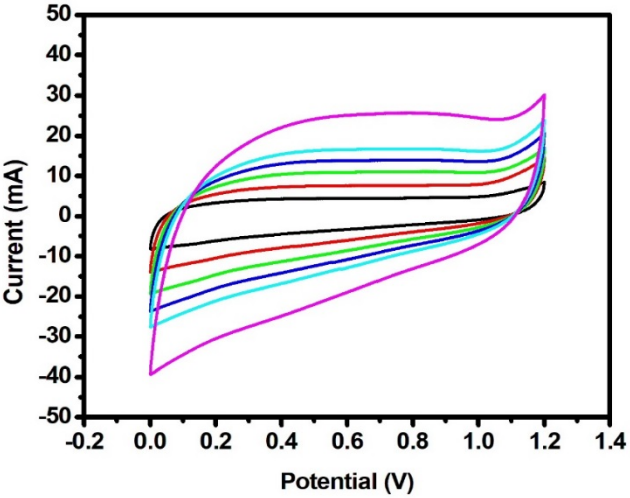

Figure 103b - Cyclic voltammogram of PB-Carbon /PVA-KOH/ Fe,Cr:$ZnCo_2O_4$ device

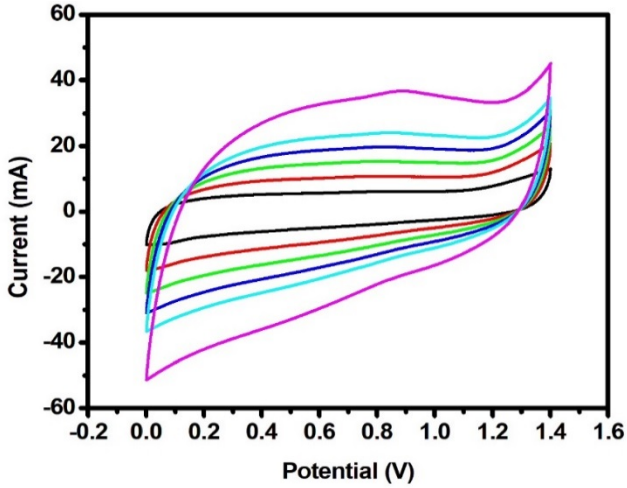

Figure 103c - Cyclic voltammogram of PB-Carbon /PVA-KOH/ Ni,Cr:$ZnCo_2O_4$ device

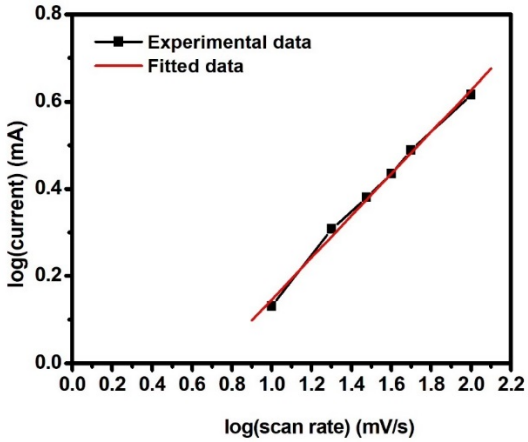

Figure 104a - Power law dependence of charge storage mechanism for PB-Carbon/PVA-KOH/$ZnCo_2O_4$ device

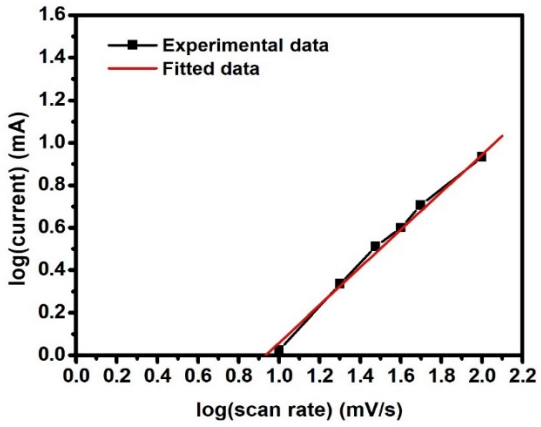

Figure 104b - Power law dependence of charge storage mechanism for PB-Carbon/PVA-KOH/Fe,Cr:$ZnCo_2O_4$ device

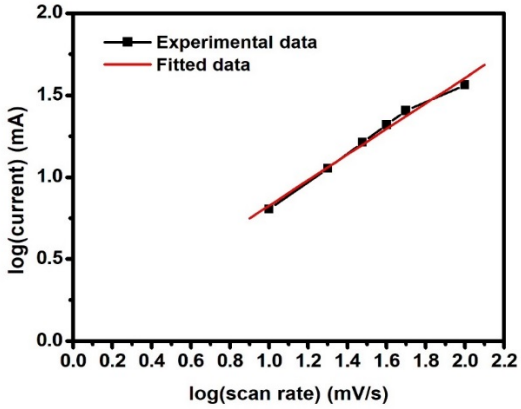

Figure 104c - Power law dependence of charge storage mechanism for PB-Carbon/PVA-KOH/Ni,Cr:$ZnCo_2O_4$ device

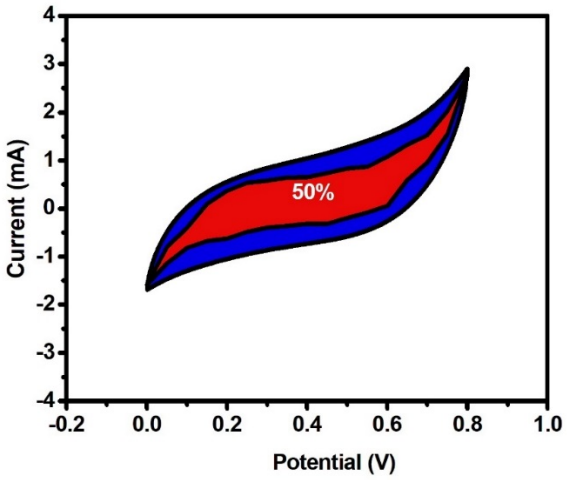

Figure 105a - Capacitive contribution of PB-Carbon /PVA-KOH/$ZnCo_2O_4$ device

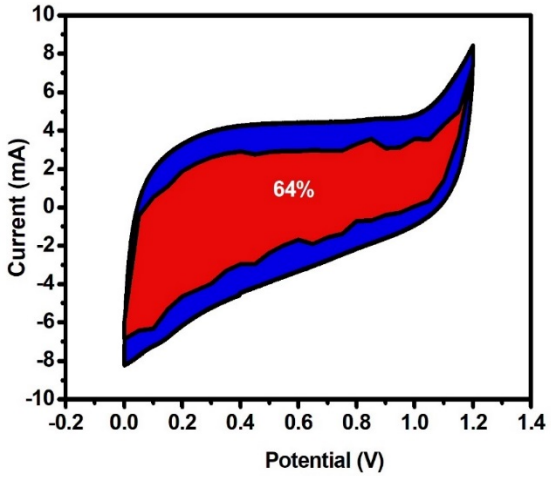

Figure 105b - Capacitive contribution of PB-Carbon/PVA-KOH/Fe,Cr: $ZnCo_2O_4$ device

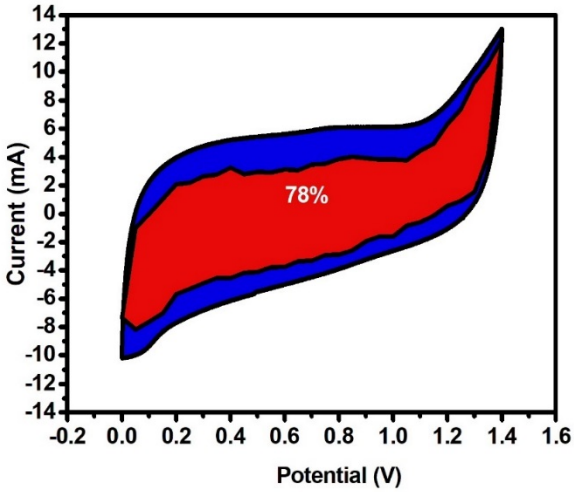

Figure 105c - Capacitive contribution of PB-Carbon/PVA-KOH/ Ni,Cr:$ZnCo_2O_4$ device

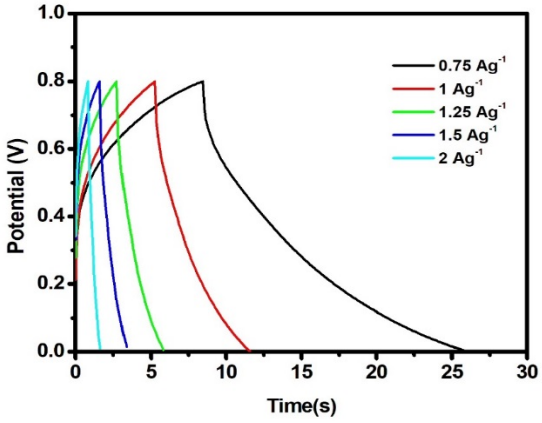

Figure 106a - Galvanostatic Charge-Discharge curves of PB-Carbon/PVA-KOH/$ZnCo_2O_4$ device

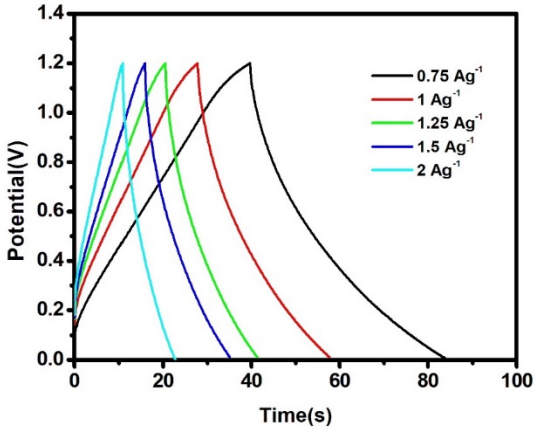

Figure 106b - Galvanostatic Charge-Discharge curves of PB-Carbon/PVA-KOH/Fe,Cr:$ZnCo_2O_4$ device

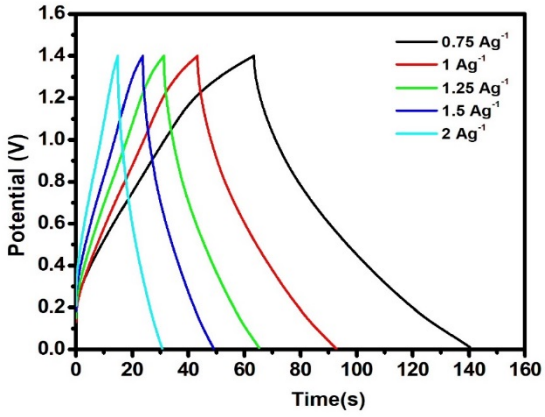

Figure 106c - Galvanostatic Charge-Discharge curves of PB-Carbon/PVA-KOH/Ni,Cr:$ZnCo_2O_4$ device

Table 52 - Gravimetric and areal performance of asymmetric supercapacitor devices of PB-carbon with undoped and doped $ZnCo_2O_4$

Device	Current density ($A\ g^{-1}$)	Specific capacitance ($F\ g^{-1}$)	Specific energy density $WhKg^{-1}$	Specific power density (WKg^{-1})	Areal capacitance ($mF\ cm^{-2}$)	Areal energy density $\mu Wh/cm^2$	Areal power density $\mu W/cm^2$
PB-Carbon /PVA-KOH/ $ZnCo_2O_4$	0.75	23.08	2.05	410.41	70.41	8.25	1251.77
	1	15.50	1.37	826.66	47.27	4.20	2521.33
	1.25	10.07	0.89	1040.32	30.73	2.73	3172.98
	1.5	7.26	0.64	1162.50	22.16	1.96	3545.62
	2	4.810	0.42	1925.00	14.67	1.30	5871.25
PB-Carbon /PVA-KOH/ Fe,Cr:$ZnCo_2O_4$	0.75	47.91	9.58	784.09	173.69	34.73	2842.33
	1	45.83	9.16	1100.00	166.14	33.22	3987.50
	1.25	41.19	8.45	1309.52	138.45	27.69	4747.02
	1.5	37.66	8.33	1554.40	151.04	30.20	5634.71
	2	32.11	7.22	2241.37	130.90	26.18	8125.00
PB-Carbon /PVA-KOH/ Ni,Cr:$ZnCo_2O_4$	**0.75**	74.23	20.20	898.14	311.78	84.87	3772.22
	1	63.83	17.37	1251.20	268.11	72.98	5255.04
	1.25	56.25	15.31	1621.32	236.25	64.31	6809.55
	1.5	50.92	13.86	1919.42	213.87	58.22	8061.57
	2	42.32	11.52	2592.50	177.77	48.39	10888.50

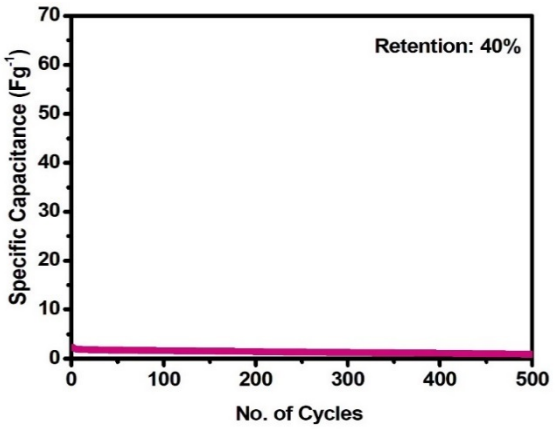

Figure 107a - Cyclic stability of PB-Carbon/PVA-KOH/$ZnCo_2O_4$ device

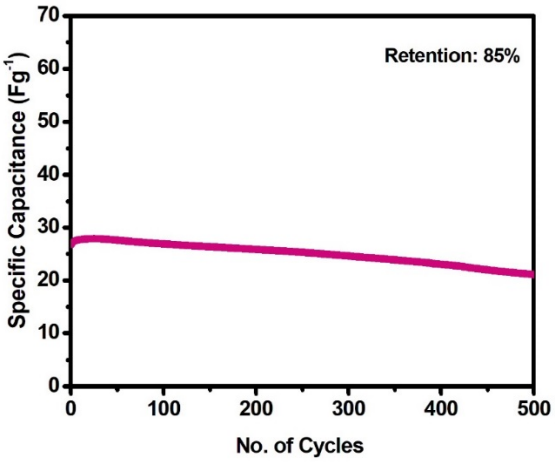

Figure 107b - Cyclic stability of PB-Carbon/PVA-KOH/Fe,Cr:$ZnCo_2O_4$ device

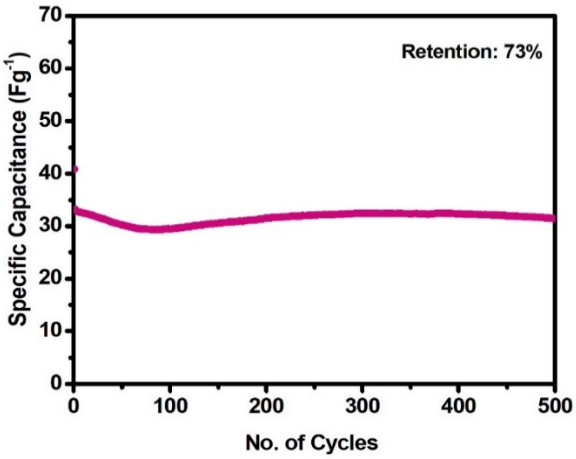

Figure 107c - Cyclic stability of PB-Carbon/PVA-KOH/Ni,Cr:$ZnCo_2O_4$ device

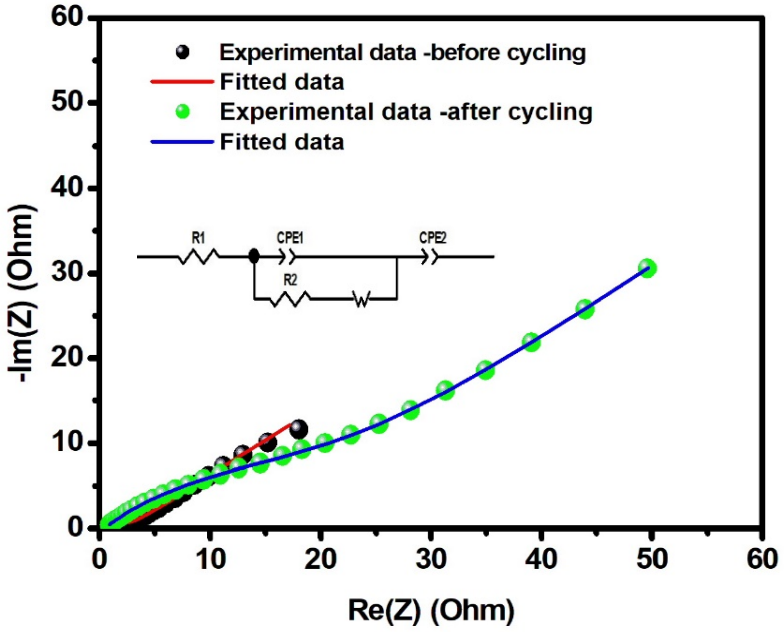

Figure 108a - Electrochemical impedance spectra of PB-Carbon/PVA-KOH/$ZnCo_2O_4$ device

Table 53 - Fitted parameters of electrochemical impedance spectra of PB-Carbon/PVA-KOH/ $ZnCo_2O_4$ device

Parameters	Before Cycling	After Cycling
$R_1(\Omega)$	0.99	0.403
$R_2(\Omega)$	0.53	19.04
CPE 1	0.60×10^{-3}	6.41×10^{-3}
n1	0.78	0.51
CPE 2	0.17	0.03
n2	0.57	0.47
W	0.12	1.13

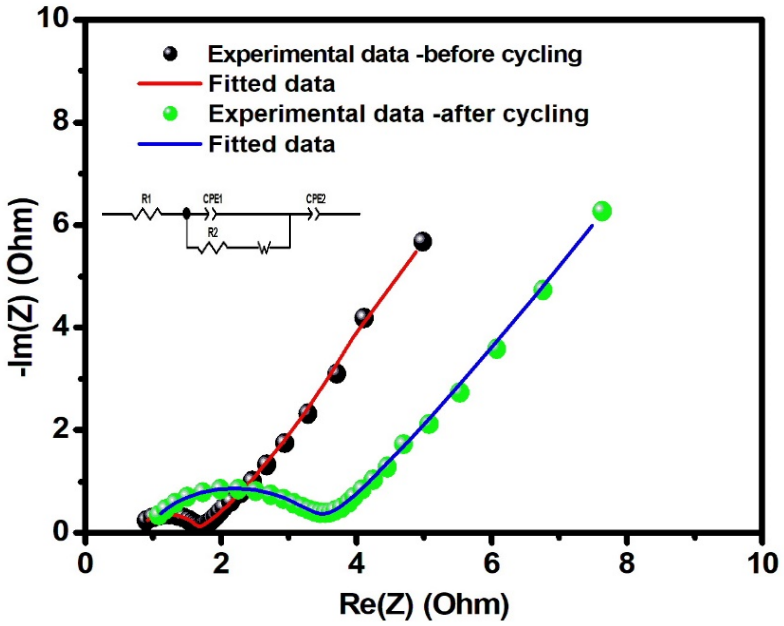

Figure 108b - Electrochemical impedance spectra of PB-Carbon/PVA-KOH/Fe,Cr:$ZnCo_2O_4$ device

Table 54 - Fitted parameters of electrochemical impedance spectra of PB-Carbon/PVA-KOH/ Fe,Cr:$ZnCo_2O_4$ device

Parameters	Before Cycling	After Cycling
$R_1(\Omega)$	0.79	0.87
$R_2(\Omega)$	0.83	2.56
CPE 1	$0.16x\ 10^{-3}$	$0.53\ x\ 10^{-3}$
n1	0.89	0.74
CPE 2	0.70	0.46
n2	0.98	0.78
W	2.24	2.41

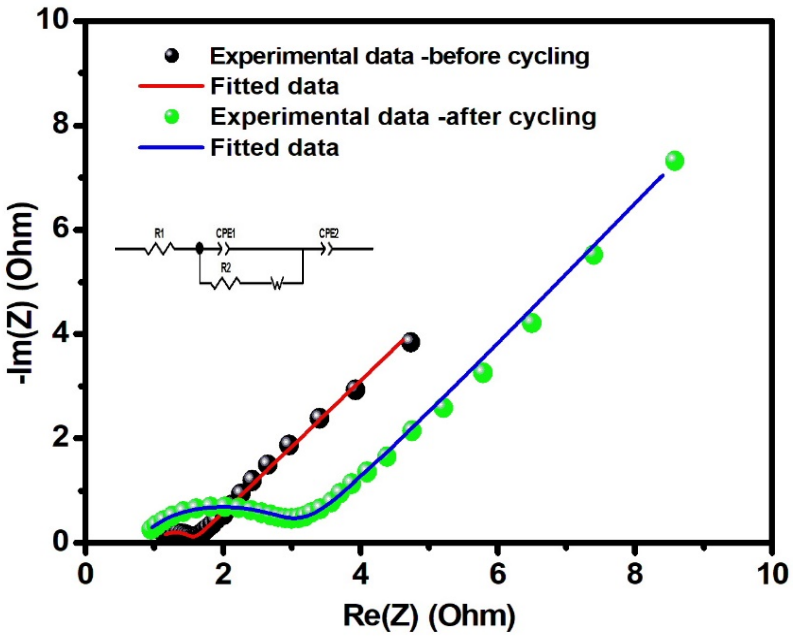

Figure 108c - Electrochemical impedance spectra of PB-Carbon/PVA-KOH/Ni,Cr:$ZnCo_2O_4$ device

Table 55 - Fitted parameters of electrochemical impedance spectra of PB-Carbon/PVA-KOH/ Ni,Cr:$ZnCo_2O_4$ device

Parameters	Before Cycling	After Cycling
$R_1(\Omega)$	0.99	0.72
$R_2(\Omega)$	0.53	2.34
CPE 1	0.60×10^{-3}	1.60×10^{-3}
n1	0.78	0.65
CPE 2	0.17	0.28
n2	0.57	0.66
W	0.12	2.36

With the detailed discussions on the performance of the devices assembled, a consolidation is done with different aspects of performance namely, (i) Specific capacitance (ii) Specific energy density (gravimetric) (iii) Specific power density (gravimetric) iv) Areal energy density and v) Areal power density. A web diagram is drawn for two different current densities of $1Ag^{-1}$ and $2\ Ag^{-1}$ and is shown in Figure 109a and 109b.

For the convenience of comparison, all the values obtained for each device is normalized in percentage and the web diagram is plotted. It obviously shows that at $1\ Ag^{-1}$ of current density, B-Carbon//Ni, Cr:,$ZnCo_2O_4$ performs better as than B-Carbon//Fe,Cr:$ZnCo_2O_4$ that are the two devices performed well. But the same device could not sustain at $2\ Ag^{-1}$. Taking into consideration of all the parameters at higher value, the B-Carbon//Ni,Cr: $ZnCo_2O_4$ is chosen for testing the flexi supercapacitor bending studies. It is also noteworthy that the S-Carbon//Ni, Cr:$ZnCo_2O_4$ show very good power density which can qualify for a hybrid functional without the demand of energy density.

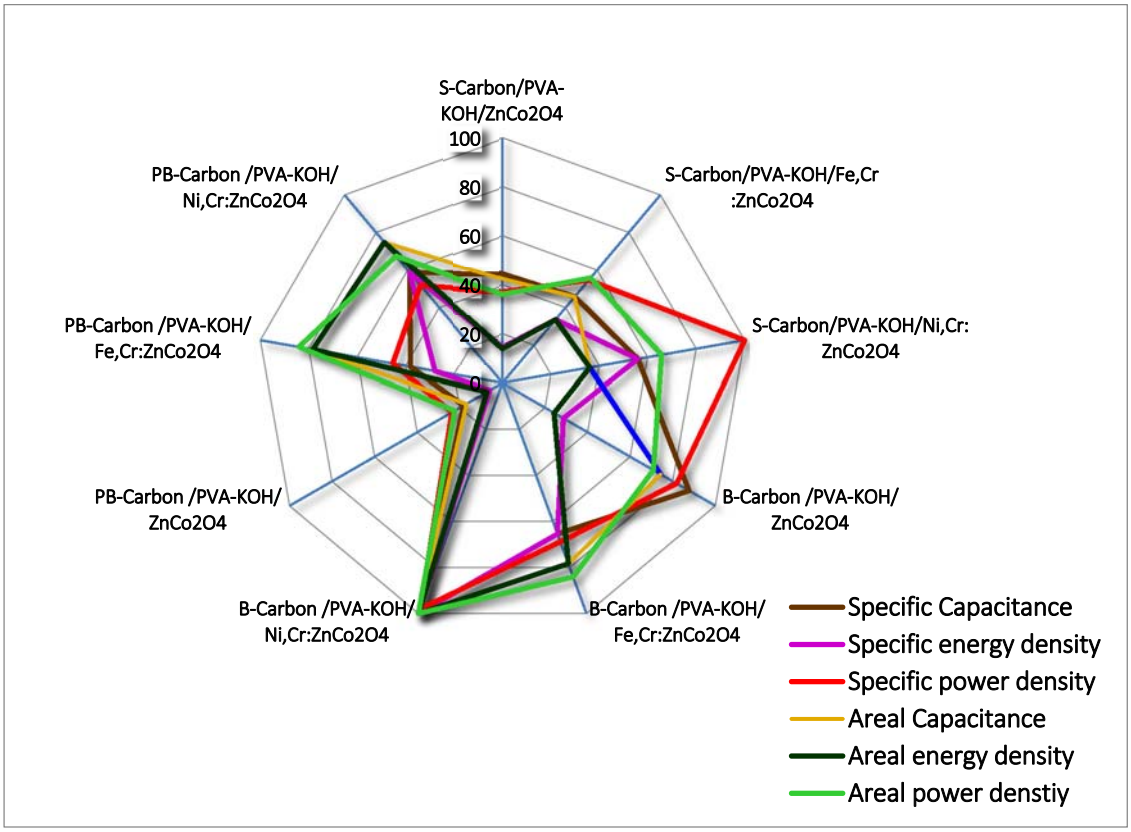

Figure 109a - Performance Comparison of all devices at a current density of $1\ Ag^{-1}$

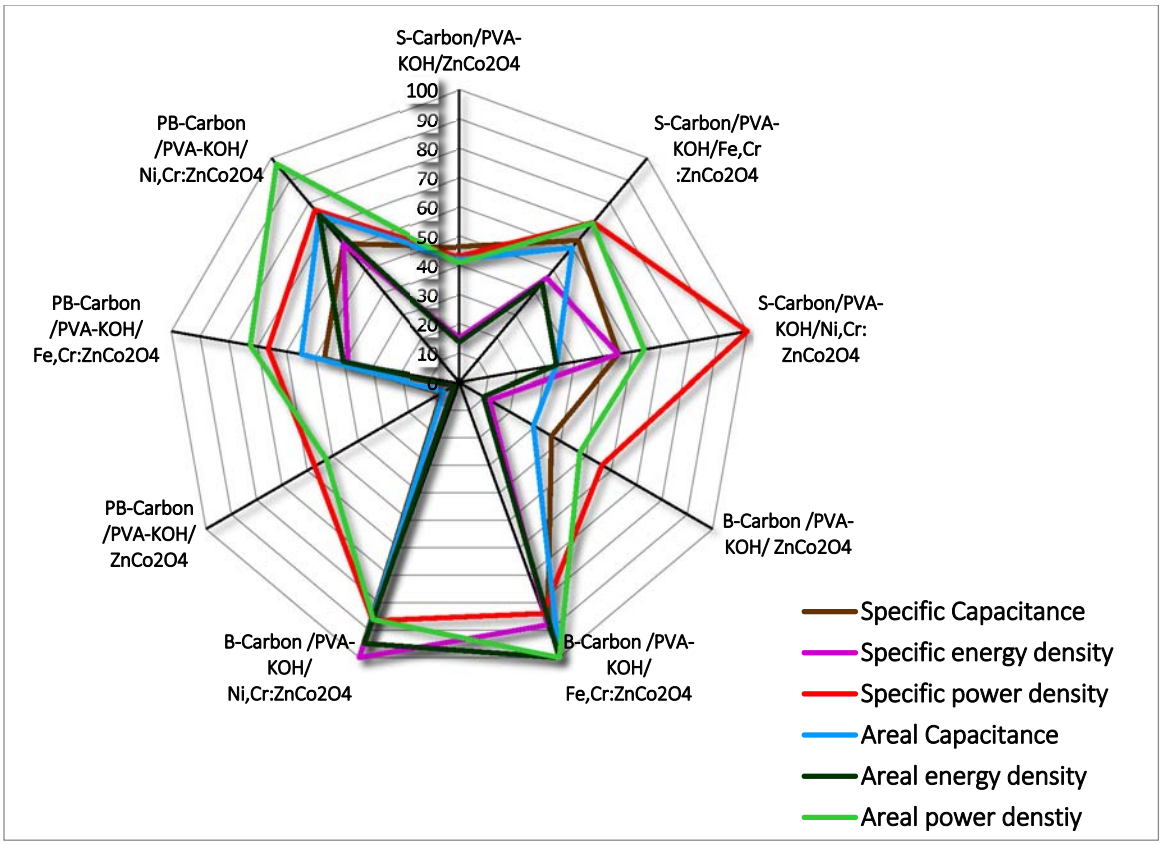

Figure 109b -Performance Comparison of all device at a current density of 2 Ag^{-1}

11.2.4. Flexible asymmetric supercapacitor

Towards testing the performance for variety of wearable devices, the asymmetric device has been analyzed at various bending states. In this case, the high performance device (B-Carbon /PVA-KOH/ Ni,Cr:$ZnCo_2O_4$) has been tested at various bending conditions. Figure 110 shows the flexibility of fabricated device. Figure 111 shows the CV curve of B-Carbon /PVA-KOH/ Ni,Cr:$ZnCo_2O_4$ at the scan rate of 100 mV/s for various bending angles such as 0° (position of as assembled device). The shape of the CV curves under different bent conditions are more or less identical, as can be shown in Figure 111. Compared to the bending state of as assembled device, the area under the CV profile is decreased while bending the device to 90°. It indicates that the associated capacitance has dropped from its initial specific capacitance. However, from Figure 111, it clear that the area of the CV curves have changed with small deviation when the bending states are progressed to 90°, 180°, and 0° (again at initial position). This implies that the capacitances

of the assembled device did not change much with bending angles. The GCD analysis is well supported by CV analysis, Figure 112. The performance parameters are calculated from GCD analysis is shown in Table 56. The specific capacitance of the device at 0° is 95.91 Fg^{-1} and it drops to 79.59 Fg^{-1} when the bending angle is reached to 90°, then it increases to 97.95 Fg^{-1} at the bending angle of 180°. Finally, it reaches to 65.30 Fg^{-1} when the device is bringing down to its initial position (0°). Hence, the corresponding energy and power density values are also changed. The change in values can be due to the better contacts achieved due to bending as seen with a typical capacitive fail in the impedance before bending and a slanted fail in the Nyquist plot after bending that has reflected in the n1 and n2 values of fitted data as well.

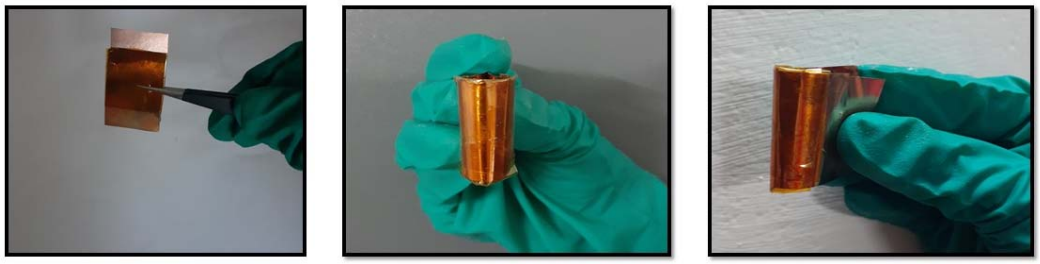

Figure 110 - Flexibility of B-Carbon/PVA-KOH/Ni,Cr:$ZnCo_2O_4$ device

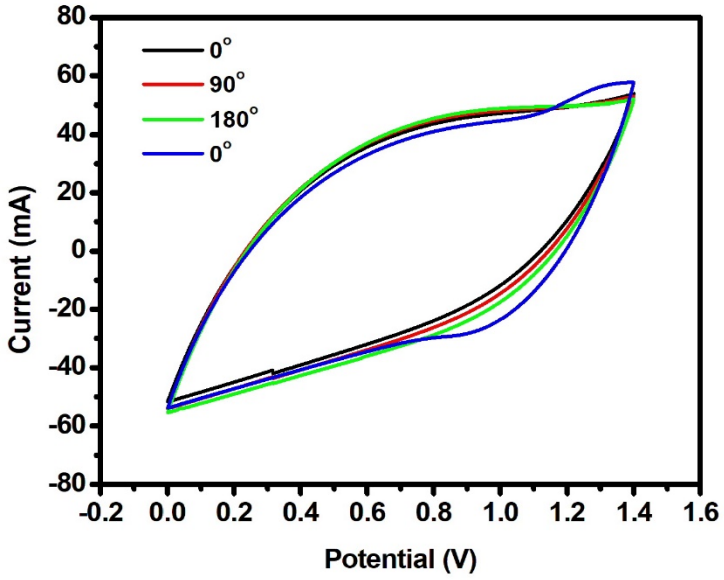

Figure 111 - Cyclic voltammogram of B-Carbon /PVA-KOH/ Ni,Cr:$ZnCo_2O_4$ device at various angles of bending at 100mV/s

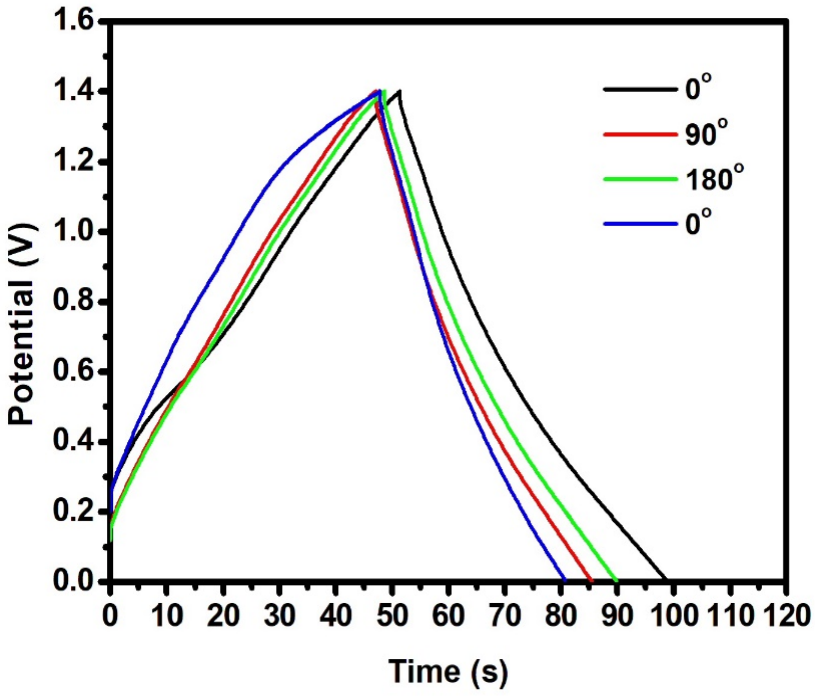

Figure 112 - Galvanostatic Charge-Discharge curves of B-Carbon /PVA-KOH/ Ni,Cr:$ZnCo_2O_4$ device at various bending states at 2 Ag^{-1}

Table 56 - Gravimetric and areal performance of B-Carbon/PVA-KOH/ Ni,Cr:$ZnCo_2O_4$ device at various angles of bending at 2 Ag^{-1}

Device	Bending states	Specific capacitance ($F\ g^{-1}$)	Specific energy density $WhKg^{-1}$	Specific power density (WKg^{-1})	Areal capacitance ($mF\ cm^{-2}$)	Areal energy density $\mu Wh/cm^2$	Areal power density $\mu W/cm^2$
B-Carbon /PVA-KOH/ $ZnCo_2O_4$	0°	95.91	26.11	3760.00	340.51	92.69	13348.00
	90°	79.59	21.66	3250.00	282.55	76.91	11537.50
	180°	97.95	26.66	3692.30	347.75	94.66	13107.69
	0°	65.30	17.77	2285.71	231.83	63.11	8114.28

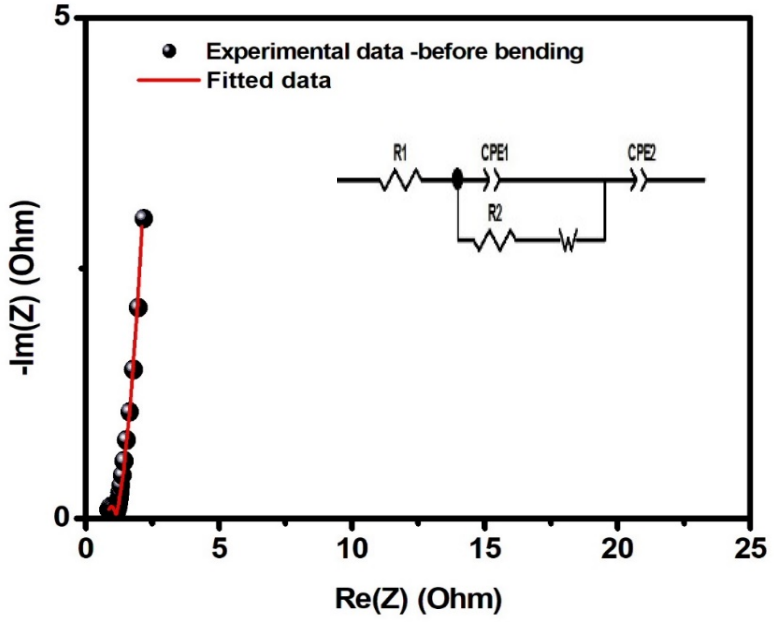

Figure 113 - Electrochemical impedance spectra of B-Carbon/PVA-KOH/ Ni,Cr:$ZnCo_2O_4$ device before bending

Table 57 - Fitted parameters of electrochemical impedance spectra of B-Carbon/PVA-KOH/ Ni,Cr:$ZnCo_2O_4$ device - before bending

Parameters	Before Bending
$R_1(\Omega)$	0.77
$R_2(\Omega)$	0.35
CPE 1	1.68×10^{-3}
n1	0.73
CPE 2	0.73
n2	0.92
W	0.59

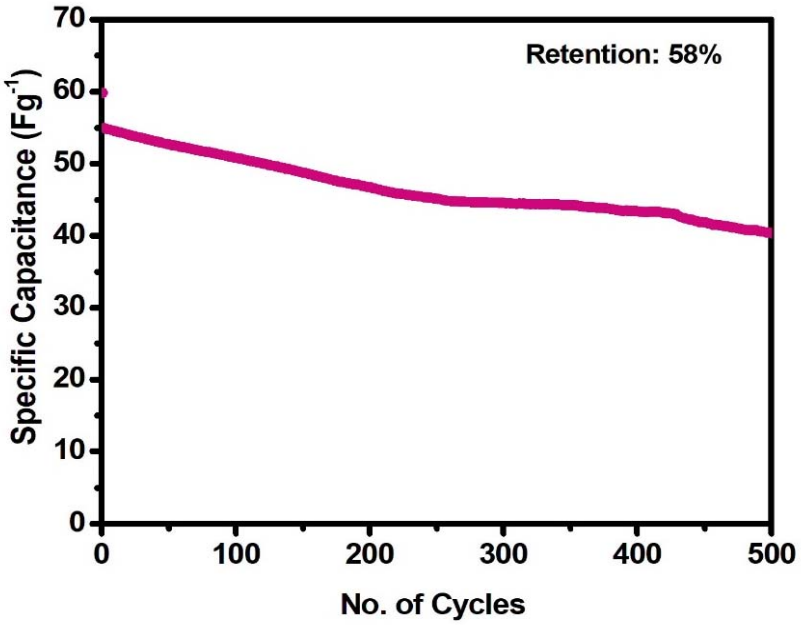

Figure 114 - Cyclic stability of B-Carbon/PVA-KOH/Ni,Cr:$ZnCo_2O_4$ device after bending

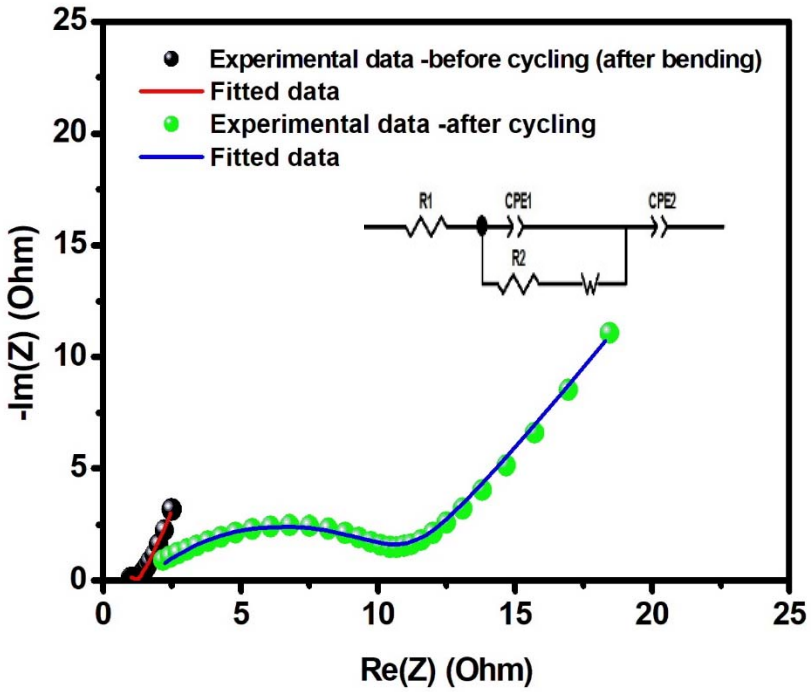

Figure 115 - Electrochemical impedance spectra of B-Carbon/PVA-KOH/ Ni,Cr:$ZnCo_2O_4$ device – before and after cycling

Table 58 - Fitted parameters of electrochemical impedance spectra of B-Carbon/PVA-KOH/ Ni,Cr:$ZnCo_2O_4$ device - after cycling

Parameters	Before Cycling (after bending)	After Cycling
$R_1(\Omega)$	1.08	1.53
$R_2(\Omega)$	1.24	9.53
CPE 1	2.10×10^{-3}	1.44×10^{-3}
n1	0.41	0.58
CPE 2	0.62	0.18
n2	0.85	0.69
W	0.52	3.07

The electrochemical impedance analysis of flexible device is shown in Figure 113. The inset shows the equivalent circuit of B-Carbon /PVA-KOH/ Ni,Cr:$ZnCo_2O_4$. The fitted parameters are given in Table 57. Before bending, the internal resistance is considerably low which get improved in on bending. Also, the spike at lower frequency is more vertical to the imaginary part which indicates capacitive behaviour of the device. The cyclic stability of the device is performed at 500 cycles after various different bending states at 3 Ag^{-1}. The capacitance retention of 58% is achieved in the case of B-Carbon /PVA-KOH/ Ni,Cr:$ZnCo_2O_4$-over 500 cycles, Figure 114. The increase in charge transfer resistance after cycling leads to capacitance loss of 42%. It is clearly seen from the Nyquist plot, Figure 115 and corresponding equivalent circuit is shown in the inset. The parameters are shown in Table 58. However, after bending there is no significant change in internal resistance. Hence, B-Carbon /PVA-KOH/ Ni,Cr: $ZnCo_2O_4$ could be suitable for flexible and portable electronic devices with improved design aspects of supercapacitors.

11.3. Summary

Out of all the fabricated asymmetric devices, B-Carbon/PVA-KOH/Ni,Cr:$ZnCo_2O_4$ assembled supercapacitor device exhibits higher gravimetric and areal performance due to the combination of high surface area anode (B-Carbon) and high specific capacitance cathode (Ni,Cr:$ZnCo_2O_4$) can be used in a single device. However, the capacitive contribution

is lower for B-Carbon/PVA-KOH/Ni,Cr:$ZnCo_2O_4$ device when compared to the device fabricated with PB-Carbon/PVA-KOH/Ni,Cr:$ZnCo_2O_4$ which may be due to the diffusive behaviour of the device. Figure 116 shows the Ragone plot of all the asymmetric devices.

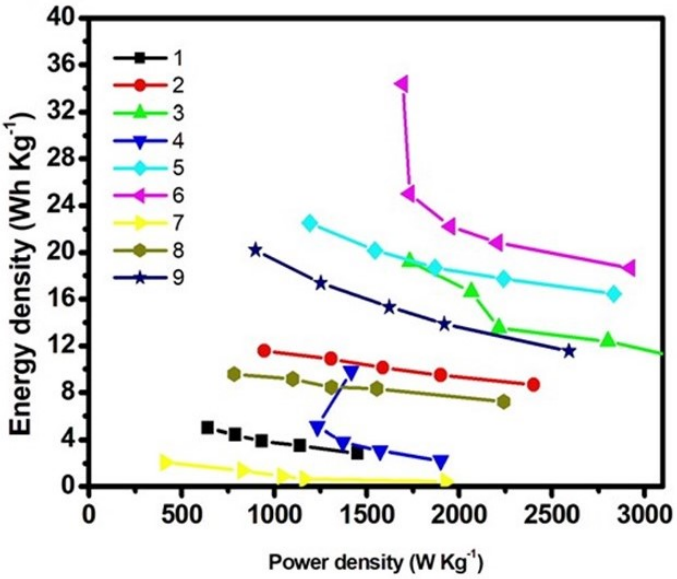

1. S-Carbon/PVA-KOH/ $ZnCo_2O_4$

2. S-Carbon /PVA-KOH/ Fe, Cr: $ZnCo_2O_4$

3. S-Carbon /PVA-KOH/ Ni, Cr: $ZnCo_2O_4$

4. B-Carbon/PVA-KOH/ $ZnCo_2O_4$

5. B-Carbon/PVA-KOH/ Fe, Cr: $ZnCo_2O_4$

6. B-Carbon/PVA-KOH/ Ni, Cr: $ZnCo_2O_4$

7.PB- carbon/PVA-KOH/ $ZnCo_2O_4$

8.PB-carbon /PVA-KOH/Fe, Cr: $ZnCo_2O_4$

9.PB- carbon /PVA-KOH/Ni,Cr:$ZnCo_2O_4$

Figure 116 - Comparison of Energy and Power density of all fabricated asymmetric supercapacitor devices – Ragone plot

From all the asymmetric device, it can be concluding that the asymmetric device fabricated with doped Zinc cobaltite exhibits better performance than pristine incorporated device. In addition, the fabricated asymmetric devices exhibit better performance than the symmetric devices which are discussed in Chapter 10.